EVALUATION OF SMALL BOWEL LUMEN FRICTION FORCES FOR APPLICATIONS IN *IN VIVO* ROBOTIC CAPSULE ENDOSCOPY

By
ALLISON B. LYLE
B.A., Communications, University of Iowa (2002)
B.S., Mechanical Engineering, University of Colorado (2012)

A thesis submitted to the
Faculty of the Graduate School of the
University of Colorado in partial fulfillment
of the requirement for the degree of
Master of Science
Department of Mechanical Engineering
August 2012

This thesis entitled:

Evaluation of Small Bowel Lumen Friction Forces for Applications in *In vivo* Robotic Capsule Endoscopy

Written by Allison B. Lyle

has been approved for the Department of Mechanical Engineering

_____

Mark Rentschler, Ph.D.

_____

Virginia Ferguson, Ph.D.

Date: _____

The final copy of this thesis has been examined by the signatories, and we find that both the content and the form meet acceptable presentation standards of scholarly work in the above mentioned discipline.

Allison B. Lyle (B.S./M.S. Mechanical Engineering)

Evaluation of Small Bowel Lumen Friction Forces for Applications in *In vivo* Robotic Capsule Endoscopy

Thesis Directed by: Professor Mark E. Rentschler, Ph.D.
Surgical Collaborator: Professor Jonathan A. Schoen, M.D.

ABSTRACT

To optimize the design of a robotic capsule endoscope (RCE) capable of exploring and delivering targeted medical therapy to the gastrointestinal tract, it is necessary to quantify the mechanical properties of the aforementioned environment. This research aims to empirically determine a coefficient of friction (COF) between the small bowel lumen and several potential RCE materials and to study how the friction response varies with velocity and contact area along the length of the bowel, specifically when eliminating edge effects from the testing coupon (sled).

To obtain friction force measurements, a novel tribometer was designed and experiments were conducted to measure the friction on the small bowel lumen surface as a function of sled speed, material, contact area, presence of a leading edge and *in situ* versus *in vitro* conditions. The friction forces ranged from 0.001 N to 0.06 N under these conditions. A dry friction model was used to extract a COF from the measured forces and COF values ranged from 0.0004 to 0.05. The results show that the COF increases with increasing sled velocity. Contact between polydimethylsiloxane (PDMS) and the intestinal lumen yields a larger COF than that of stainless steel or polycarbonate. The COF does not demonstrate significant changes with pressure, but does respond to changes in contact area and weight, although the complexities of that relationship were not thoroughly investigated in this research. The results also indicate that by eliminating edge effects, the friction force between a stainless steel sled and the small bowel lumen surface is decreased. The average COF for *in situ* testing was found to be slightly lower than *in vitro* tests. These results can be incorporated into the design and control of an RCE to improve mobility within the gastrointestinal tract.

ACKNOWLEDGEMENTS

I would like to thank Dr. Rentschler for his endless encouragement, guidance and patience. His belief in my potential as an engineering student was vital to my success. I would like to thank Dr. Schoen for his time and surgical expertise. Thank you to Ben Terry for being an excellent mentor and steward for proper research in engineering. Thank you to Dr. Luftig for his unparalleled expertise in research statistics and for his time and willingness to ensure that any student who desires to learn deserves as much time as he can afford. Thank you to all of the members of the Advanced Medical Technologies Laboratory for their kindness, support and friendship. Finally, thank you to my amazingly supportive parents, to Andy and to the rest of my family for doing everything and anything they could to encourage and empower me while pursuing this goal.

Contents

List of Tables

List of Figures

Chapter 1

Introduction

Capsule endoscopy (CE) is an effective diagnostic technology employed within the gastrointestinal tract which can be further enhanced by improvements in mobility. Robotic capsule endoscopes (RCEs) offer the promise of improved control and positioning, which will lead to diagnostic and remedial benefits for the patient and physician. In order to optimize the design of a RCE capable of maneuvering within the bowel, it is critical to characterize the mechanical properties which will affect the RCE's movement. In this work, we provide measurements of the friction force between the small bowel lumen in contact with assorted engineering materials as a function of speed, pressure, contact area, region of the bowel, edge effects and tissue conditions. These results show that the friction response of the tissue is a complex phenomena with interactive dependencies upon all of the aforementioned parameters. With this information, it will be possible to make design selections to optimize the friction response between an RCE and the small bowel surface as required for mobility.

1.1 Motivation

Over 60 million people in the United States are affected by gastrointestinal (GI) disease, with nearly half of those diseases metastasizing in the intestinal tract [1]. Diseases such as Celiac and Crohn's disease, intestinal cancer, peptic ulcers, polyps and a host of other chronic intestinal problems can often be treated successfully if identified and attended to as quickly and properly

as possible. Radiographic imaging is only marginally effective at indentifying these diseases and has been replaced with improved endoscopic and enteroscopic tools [2]. The drawbacks to the latter procedures include patient discomfort, risk of intestinal wall perforation, time and costs associated with sedation and the length of tethered scope [3]-[6]. As a result, capsule endoscopes have been developed for improved access and semi-autonomous use. A commercially available capsule endoscope, named the PillCam, is a passive diagnostic tool which can be swallowed by the patient and has been shown to be effective in a number of studies [7]-[11]. The PillCam makes use of an on-board camera to take images of the small bowel several times per second as it moves aborally via the peristaltic contractions of the bowel. The challenge with these types of devices is their passive translation and the inability to track specific position relative to the length of the bowel.

In order to improve the effectiveness of existing capsule technology, a number of research groups are pursing the goal of developing Robotic Capsule Endoscopes (RCE)s. RCEs may have the ability to perform tasks such as imaging, biopsies and targeted drug delivery that are not possible with the procedures and equipment available today [12]-[15]. For an RCE to be effective, it must be able to independently maneuver within the gastrointestinal (GI) tract, which includes controlling its position, speed and direction. For the capsule to perform desired tasks, it must be able to hold or reverse its position as the peristaltic contractions of the small intestine naturally force the device aborally. The capsule must therefore overcome two primary hindrances: 1) the lack of adequate reaction forces from the intestinal wall, and 2) low friction on the mucosal surface. Mobility will also be affected by changes in the chemical and mechanical structure of the mucosal surface, which are known to vary significantly in this region [16]. To properly design an RCE with the ability to traverse these surfaces, it is essential to quantify the

physical and mechanical properties along the length of the small bowel. To optimize mobility, it is necessary to understand the parameters which can be manipulated to maximize or minimize surface friction interactions as desired. In order to better understand the challenges associated with motion control, it is helpful to consider the complex environment of the small bowel.

1.2 Anatomy of the Gastrointestinal Tract

The GI tract is composed of the esophagus, stomach, small and large bowel and the anus [17]. For the purposes of endoscopic capsule movement, a focus is placed on the small bowel for several reasons: 1) it has the smallest diameter of the entire tract, 2) it is the longest portion and least accessible portion of the tract, averaging 4.6 m long and consists of many folds and curves, which create mobility challenges for an endoscopic capsule to overcome as well as accessibility issues for surgical tools and scopes and 3) pathologies within the small bowel manifest in ways that affect vital nutrient absorption [17],[18]. The small bowel is divided into the duodenum, jejunum and ileum, with each performing different roles in the digestive process. The duodenum is most proximal to the stomach and is the first to receive its contents, which are then mixed with digestive juices secreted by the gall bladder and pancreas [17]. The first few centimeters also contain Brunner's glands, which secret alkaline mucus that, along with pancreatic enzymes and bile, protect the tissue from the acidic digestive juices. As the contents travel through the distal small intestine, they become liquefied as they join with water, mucus, bile, and pancreatic enzymes. The food to be digested is mixed as the muscles of the intestinal wall alternately contract and move it towards the jejunum, where the majority of digestion and nutrient absorption takes place. The ilieum absorbs any remaining nutrients into the blood stream before the waste is moved towards the ascending colon [19].

The heterogeneous structure of the small bowel is complex, as shown in Figure 1 [20]. The major tissue layers consist of the serosa, which is the outer most surface connecting to the mesentery, longitudinal and mutually orthogonal circular muscle layers, the submucosa and the mucosa. The diameter of the small intestine varies along its length, ranging from 2.5 cm in the ileum to 3.5 cm in the jejunum [17]. The thickness of the intestinal wall also differs, ranging from 1 mm to 3 mm, excluding the mucosal layers. Extending from the mucosal wall toward the lumen are small flexible columns, called villi, from which additional smaller columns extend, termed microvilli. The purpose of these flaccid structures is to aid in mixing and to increase the surface area of the intestine to aid in nutrient absorption.

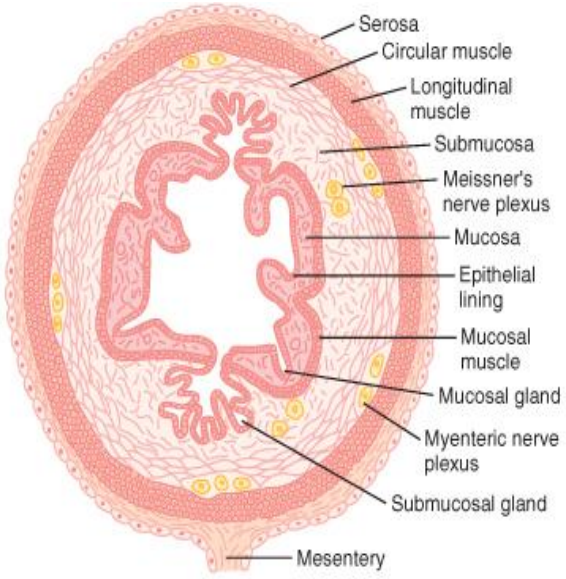

Figure 1. Cross section of the bowel [20]

Within the various folds of the villi and coating the intestinal surface is a film of mucus which is secreted by local goblet cells and comprised of two layers, as shown in Figure 2. The firmly adherent layer serves to protect the underlying mucosa, while the loosely adherent layer acts as a lubricant to allow smooth passage of the contents being digested. The bulk mucus is comprised of primarily water and mucin glycoproteins, along with DNA, various other proteins, lipids, salts, cells and cellular debris [21].

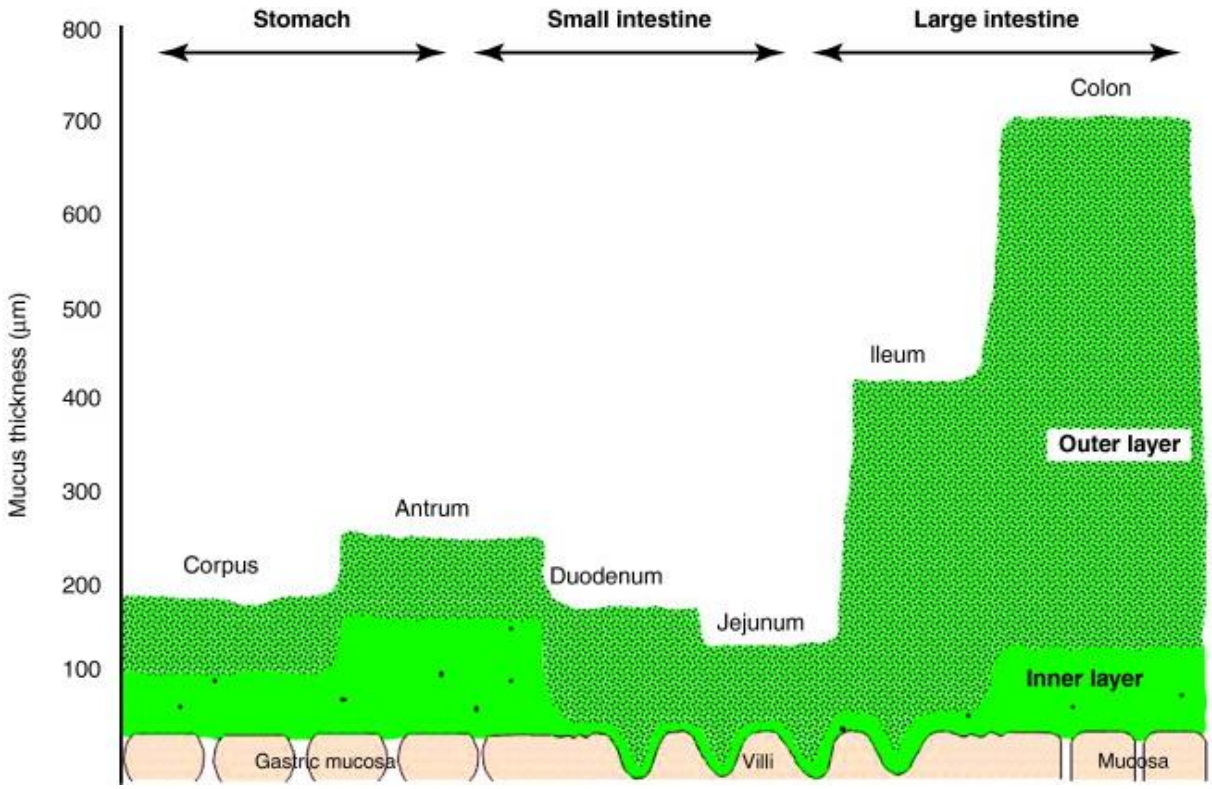

Figure 2. Mucus thickness along the length of the GI tract [22]

1.3 Robotic Capsule Endoscopes (RCEs) in the Small Bowel

Not only are the surface interactions with the bowel surface complex, an RCE must also overcome a variety of forces which will be working to move the capsule along the length of the GI tract. These forces include the peristaltic wave contractions ($F_{\text{mechanical}}$) and myenteric contractile forces ($F_{\text{myenteric}}$) from the intestinal wall, as well as mucoadhesion ($F_{\text{mucoadhesion}}$), or the energy required to separate the collapsed lumen and friction between the capsule surface and intestinal wall [23]. The surrounding organs, weight of the intestinal wall and pressure from the fluid within the bowel also impart forces on the RCE, in addition to gravity, which acts as a body force ($F_{\text{abdominal}}, F_{\text{hydrostatic}}, F_{\text{RCE weight}}$, respectively). Friction forces, including dry contact between the tissue and RCE surface ($F_{\text{dry friction}}$) as well as fluid shear ($F_{\text{fluid shear}}$), act

in opposition of the RCE's movement. A schematic of the primary forces acting against a theoretical RCE is shown in Figure 3.

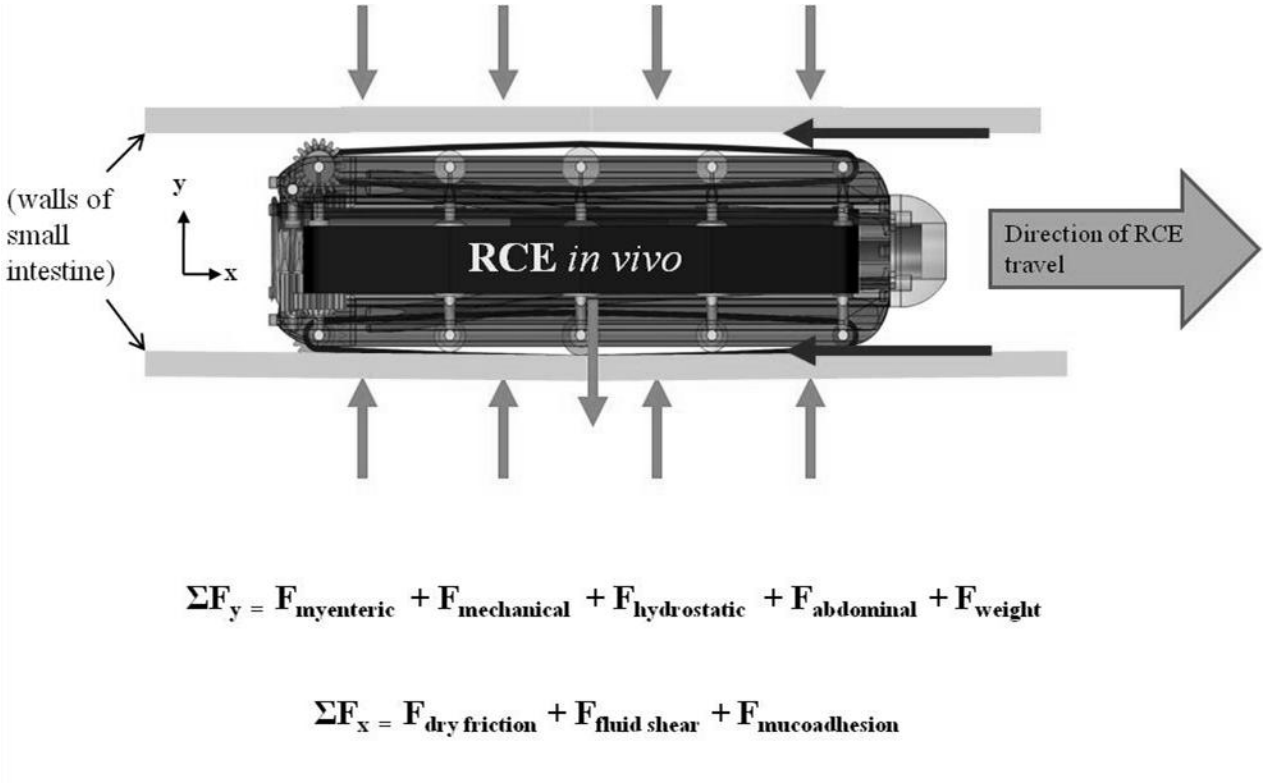

Figure 3. Simplified free body diagram of RCE *in vivo,* depicting the primary forces from the small bowel acting both normal to and in opposition to the RCE's movement.

Experimental data relating to the aforementioned measured forces is somewhat limited and is primarily obtained under *in vitro* conditions [23]-[31]. Biaxial stress measurements have been collected as well as myenteric contractions and show small bowel to be viscoelastic with time dependent stress and strain [23]-[26],[30]. Friction forces have also been measured, however, the published values are highly variable based on a number of parameters, such as the material in contact with the tissue, capsule geometry and weight, contact area and speed [28],[30],[32],[33]. Friction manipulation is currently one of the primary obstacles to initiating and controlling endoscopic capsule movement. Knowledge of the static and dynamic friction

forces that the robot will encounter during initiation of movement and subsequent locomotion is of utmost importance. It is the frictional properties of this mucosal surface that this research intends to examine.

1.4 Tribology

Tribology, or the study of surface characteristics and interactions, is a necessary component for understanding mobility within the small bowel. Tribometry tests can be performed in a number of ways, with the two most common approaches involving: 1) pulling a sled of known material across a surface, or 2) by a pin-disc system, where a rounded head is pressed against a surface specimen on a rotating disc. The force required for the two materials to move from a static to dynamic state is measured.

For two rigid, unlubricated surfaces, the friction force can be characterized by three dry friction laws, summarized in (1). Amonton's first law states that the friction force is directly proportional to the applied load [34],[35]. Amonton's second law and Coulomb's law state that the friction force is independent of contact area and velocity, respectively. Amonton's law can be rearranged to determine a dry friction coefficient, μ, by dividing the measured friction force, F_f, by the normal force being applied, F_W, shown in (2).

$$\boldsymbol{F_{dry\ friction}(F_W, V, A_c)} = \begin{cases} \boldsymbol{\mu F_W}, & \boldsymbol{F_N \geq 0} \\ \boldsymbol{\mu F_W}, & \boldsymbol{V \geq 0} \\ \boldsymbol{\mu F_W}, & \boldsymbol{A_c \geq 0} \end{cases} \tag{1}$$

$$\boldsymbol{\mu} = \frac{\boldsymbol{F_f}}{\boldsymbol{F_W}} \tag{2}$$

Additional friction models exist across a spectrum of varying complexity, ranging from these basic friction laws to complex friction models which account for velocity, weight, contact

area, temperature, presence of a lubrication layer and mechanical properties specific to the materials in contact [34],[36]-[41]. Unfortunately, these models are not able to account for the unique surface structure of the intestinal tissue, nor the mucus layer which coats the lumen surface. Like most biological tissue, intestinal tissue is non-homogenous, anisotropic and viscoelastic and its properties can vary significantly based on its condition of hydration, blood supply and temperature, among others. According to Laio, *et al*, the GI tract must be studied as a multi-layered composite material, made up of tissue with different mechanical characteristics [42]. The tissue surface is complex on its own and friction behavior is further complicated by the addition of a viscous mucus layer. Lai, *et al* defines the bulk mucus layer as a viscoelastic gel which possesses behavior similar to an elastic solid at low shear rates and reverts to viscous fluid behavior at high shear rates [43]. Mucus is considered to be a non-Newtonian fluid up to a certain shear rate, beyond which it can be considered Newtonian [43]-[45]. The rheological properties of mucus secretions have been shown to be equivalent throughout the GI tract (from duodenum to colon) [43]. However, the viscosity is sensitive to physiological and pathological changes, which is important to consider when designing an RCE being used for diagnostic purposes [46].

Olsson, *et al* noted that in systems with a lubrication layer, the COF normally decreases with increasing velocity, with an exception being when the lubrication layer is considered large enough so that the opposing bodies do not come into contact, where dry friction submits to hydrodynamic effects and the COF increases with increasing velocity [36]. Grosch suggested that for viscoelastic materials at low velocities, friction coefficients can be considered to be totally independent of velocity [37]. That threshold of course, is material dependent. Beyond that threshold, at a fixed temperature, friction coefficients increase with increasing velocity, however

Grosch has suggested that there is a maximum COF that can be reached, after which the friction coefficient decreases despite increasing velocity. Rubber in contact with a rigid surface has been studied most commonly, and it has been suggested that a “master curve” can be developed to describe resistance forces as a function of temperature and velocity. This velocity dependence of friction is attributed to the rate-dependent strength of adhesive bonding that occurs.

Gong, *et al*, noted that polymeric gels exhibit friction forces with complicated velocity and load dependencies, based on whether the two materials in contact demonstrate adhesive or repulsive behavior [41]. In the repulsive case, the friction force is proportional to the increase in velocity. In the attractive case, the friction force would reach a maximum with increased velocity. The chemical structure (i.e., polymer network) and solvent content of the gel are substantial factors in the friction response, as they can demonstrate adhesive or deformation characteristics or alternatively, serve as a lubrication layers. Gong *et al* also found that friction behavior of polymeric gels is "strongly dependent" on the (apparent) contact area of the two surfaces and went further to suggest that the "friction force per unit area is related with the normal pressure, instead of the load [41]."

Because of its complex nature, friction models specific to the small intestine surface are sparse. Given the complex behaviors of the surface interactions within the small intestine, Amonton’s basic friction model may overestimate the friction coefficient; however, it is an appropriate starting point from which future models can build. It is helpful to consider models that describe the friction behavior of viscoelastic materials and viscous gels and use those conclusions when forming a hypothesis.

Chapter 2

Literature Review:
Experimental Evaluation of Small Bowel Friction Forces

There are a number of research groups with the same goal of modeling the gastrointestinal tract, several of which have produced experimental data reporting friction forces and coefficients. The challenge in interpreting and utilizing the existing results is the multi-variable dependence of friction forces involving a viscoelastic surface. Specimen preparation, condition and temperature as well as the weight, contact area, geometry, material and velocity of the surface interacting with the mucosal surface all contribute in varying and somewhat inconclusive degrees. Thus, different research groups have made different conclusions as to the effect each of these variables have on the friction force and resulting coefficient of friction.

The following sections detail the findings of those who have focused their testing on the friction behavior of the small intestine. To start, research groups who have performed experiments on open and closed small bowel specimens will be reviewed, outlining the results based on the independent variable being manipulated. Friction coefficients will be compared when available, supplemented by friction force values when not.

2.1 Open Specimen Tests

Yoshida, *et al* investigated the tribological properties of many living tissues, specifically considering the effect of hydration [33]. Small intestine samples, which had previously been

frozen, were brought to room temperature and placed on a rotating disc, which rotated within a saline filled vessel. For the first experiment, a friction coefficient was obtained for three intestinal surface conditions: a) intact, meaning that the surface was in its untreated state, covered with food from digestion, b) softly wiped with gauze, and c) rubbed with gauze so as to remove the surface layer. The sliding speed of the ceramic face against the intestinal specimen was 20 mm/s and the mean contact pressure was 12 kPa. The friction coefficient results were plotted as a function of time from 0 to 800 seconds. All tests showed an increasing COF over time, with the hard wiped surface resulting in the largest friction coefficient, reaching a maximum of 0.24. The intact surface yielded the second largest maximum COF at nearly 0.18, and the maximum for the soft wiped surface was approximately 0.06.

Yoshida also considered the effect of sliding speed on friction, testing at speeds of 5, 10, 20, 40 and 80 mm/s. The friction coefficient was again shown plotted over a time interval, in this case 600 seconds, during which case the COF value increased. The results show a clear relation between increasing speed and subsequent increase in friction coefficient. At speeds of 5mm/s, the friction coefficient increased slowly with time and remained below 0.05 [33].

Yoshida considered the water content to be the primary factor affecting the coefficient of friction, stating, “Under a load, water exudes slowly from the surface layer with or without sliding. As a result of the water loss, thickness of the surface layer reduces and water content of the surface layer decreases. Consequently, the degree of adhesion to the upper specimen increases and frictional force increases. Therefore, it may be concluded that friction depends essentially on water content of the surface layer [33].” Regarding the effect of velocity on the friction force, the authors concluded, “Since the fluidity of the water absorbed by the layer is low, it can lubricate the surface as well as a highly viscous fluid can, even if the sliding speed is

low." They generally noted that, "The surface layer seems to have the ability to recover the condition of low friction."

N.K. Baek, *et al* performed experiments to gather friction forces for capsules of various sizes and contact areas made of both aluminum and acetyl plastic [28]. Tests were performed on open specimens of small intestine maintained at 37° Celsius and maintained at a pH between 7.4-7.8. An isotonic saline solution was sprayed over the intestine to maintain hydration. Both open and closed specimen tests were performed for comparison. For the open specimen test, an aluminum capsule with a radius of curvature of 2 mm was pulled along an open specimen at a velocity of 0.5 mm/sec. The actual diameter, length and contact area were not provided for this capsule, although it was selected from a group of capsules that underwent testing within a closed intestinal specimen with diameter between 7-10 mm and of length between 15-25 mm. The average friction force over measured over the distance of 50 mm was 5 mN, approximately four times smaller than the average force measured in the closed specimen. The authors attributed this reduction to the absence of a circumferential viscoelastic force, which contributes to the total normal force of the capsule in the closed specimen.

J.S. Kim, *et al* published results evaluating the effect of normal load, contact area and velocity on the friction force and friction coefficient [30]. During these tests, the intestinal specimen was held at 36.5° C, and a pH level in the range of 7.4-7.8 was maintained. Five aluminum blocks of varying weight were compared for the tests, with each having identical contact area of 502.4 mm^2 and radius of curvature of 2.0 mm. The weights ranged from 40.2 mN to 322.42 mN. The blocks were pulled across the intestine surface at speeds between 0.16 and 0.5 mm/s (actual speed increments not reported). With increased normal force, the friction force increased accordingly, however the friction coefficient decreased. The friction forces increased

from approximately 8 mN to 27 mN across the aforementioned weight range and the friction coefficient decreased from 0.2 to 0.07. Kim's group surmised that this was due to the "squeezing" of liquid from the intestinal surface, which served as a lubrication layer between the block and the intestine surface.

J.S. Kim's group then compared five aluminum blocks of varying contact areas across the intestinal specimen at the conditions noted above. These blocks varied in their contact areas from 502.4 mm^2 to 1758 mm^2 and were all of the same weight of 252.8 mN. This experiment showed no significant variation in friction force, and hence friction coefficient, with changes in contact area. They concluded that "the surface area of the capsule does not need to be considered for the capsule design from the tribological viewpoint." This conclusion was contrary to closed specimen capsule testing results that indicated a possible dependence of friction force on contact area, to be described in the following section.

Y.T. Kim *et al* performed experiments to measure the friction force of acrylic plastic and steel cylindrical sleds placed vertically (providing a circular contact area) on an open small intestine [47]. Two plastic cylinders 2 mm in diameter were fabricated, one of which was solid and one was hollow. The inner diameter of the hollow cylinder measured 1.2 mm. Two steel sleds of 6 mm diameter were also tested, one solid, one hollow. The inner diameter of the hollow steel cylinder was 5.4 mm. The use of different materials were justified by referencing Baek's work, which did not find a large difference in the friction forces yielded by plastic and aluminum when tested in a closed specimen. All four cylinders weighed 2 gf and traveled a distance of 100 mm at a rate of 10 mm/s. The average friction force for the hollow plastic cylinder was 1.2 gf, compared to 1.5 gf for the solid cylinder. The steel sled yielded different results, with the hollow cylinder registering a higher average force of 1.5 gf, versus 1.0gf for the solid cylinder. The

group reported a friction coefficient in the range of 0.5-1.3, noting that the large range was attributed to local, instantaneous friction increases over the course of travel.

Y. T. Kim's group concluded, "The frictional force generation is due to a combination of mechanical interlocking and sliding friction on the flat bottom part of the cylinder specimen. The mechanical interlocking occurs at the outer boundary of the cylinder in the case of the solid cylinders [47]." The solid 6 mm cylinder had a lower friction force than the 2 mm cylinder, leading the authors to conclude that frictional force between a solid material and the small intestine is independent of apparent contact area. The major difference between hollow and solid was due to the protrusion of intestine at the center of the hollow cylinder. This protrusion was insignificant for the inner diameter of 1.2 mm for the 2 mm capsule, but was notable for the 6 mm hollow cylinder with inner diameter of 5.4 mm.

In their work published in 2009, Y.T. Kim's group evaluated friction forces between the small intestine and various configurations of rigid and flexible tubes with different tip configurations [48]. Two flexible polymeric tubes with flat and ball shaped tips were tested against two rigid acrylic rods of flat and ball tips, each of which was reported to weigh 2 gf. The ball was made of steel with an unknown diameter. The tests were performed within five to seven hours of slaughter and excision from the porcine donor and the intestinal samples were wetted with saline solution throughout the testing. Each object was tested three times, all on the same sample, which was placed on a water bag while the testing objects were slid upon it so as to simulate the compliant reaction forces of surrounding tissues in the abdomen. The sliding velocity was fixed to 5mm/s.

Friction coefficients were calculated for each of the four testing configurations using a standard dry friction equation. The rigid flat tip was found to produce the lowest friction

coefficient of 0.52, followed by the rigid ball tip at 0.84 and flexible ball tip at 0.85. The flexible flat tip produced the highest friction coefficient at 1.17. The results also showed a repeatable friction behavior over the length of the specimen that indicated an effect from the intestine's surface geometry and structure.

In this publication, the authors noted that, "As the contact moves in the horizontal direction, a combination of sticking and sliding phenomena occur…The degree of sticking depends on the frictional interaction between the tip and the intestine as well as the tissue structure of the intestine surface, which is not uniform [48]." A significant and repeatable friction effect is produced from the surface geometry and structure of the intestine, as is evidenced from overlaid plots of the friction force over the travel distance. The equivalent COF values for the ball tip on both the rigid rod and flexible tube were due to the negligible change in contact geometry when the flexible tube complies with the friction force from the intestine. (The exact diameter of the ball was not reported, but visually appeared to be just under 2 mm).

Xiaona Wang, *et al* also evaluated friction forces on both open and closed small bowel specimens, specifically as a function of weight, velocity and capsule dimension [32]. For the open specimen testing, two blocks of ABS plastic were utilized, with contact areas of 750 mm^2 and 1380 mm^2, however their aim was not to evaluate the effect of contact area on friction for the open specimen study. The blocks were pulled at a speed of 0.5 mm/s over a splayed specimen resting on a large water tank maintained at 37 °C. The test was run on two specimen samples, each sprayed with a physiological saline solution to preserve the integrity of the sample. Measurements were taken every four seconds and a single force measurement was calculated by averaging 30 measurements. The friction force for block 1, with contact area 1380 $mm^2$was evaluated with weights ranging from 15 g to 35 g, incremented by 5 g, and was found to increase

by 20 to 30 ±5 mN. Block 2 was tested with weights between 5 g and 35 g, also incremented by 5 g, and the friction force increased by 20 to 40 ± 5 mN. The friction coefficient was approximated to be on the order of 10^{-1} and it was concluded that the effect of weight on friction force was negligible. This conclusion was based on the weight of the capsule being less than 5 g.

X.Wang then considered the effect of speed on friction force by testing block 1 at speeds of 0.5, 3, 5 and 8 mm/s on one specimen sample [32]. Weights of 20, 25 and 30 g were tested. The increase in force was by approximately 100 to 130 ±12 mN for velocities of 0.5 to 8 mm/s, which was significantly larger than the effect of weight on resistance force. However, when comparing the results acquired from the previous tests to determine the effect of weight on the friction force, Block 1 with weights of 20, 25 and 30 g and traveling at 0.5 mm/s produced friction forces that were nearly 2 times higher than the forces reported for block 1 traveling at 0.5mm/s for the velocity comparison tests. The tests for the weight comparisons were performed on two different intestinal specimens, and it appears that the test for the velocities may have been performed on a third specimen sample. Wang noted that the 'startup' force for the capsules in the closed intestine was greater than that for the blocks on open specimen, due to prominence of viscoelastic properties of tissue. The large startup force for blocks was deemed to be a result of mucus substance flow in front of the sharp leading edge.

Finally, K.D. Wang, *et al* tested the effect of weight, material and geometry on the friction force and friction coefficient [49]. The intestinal specimen (from an unknown location in the bowel) was extracted and flushed with saline after the animal was killed. Eight sleds with varying surface areas and contours were pulled across the specimen while weight was changed "continuously." Two flat sleds were used in the testing, one made of copper and one of

aluminum, each with surface area of 35 x 35mm. The speed of travel was not reported. The normal force for the aluminum sled was increased from 9.6 to 109.6 gf and the normal force for the copper sled was increased from 28.3 gf to 128.3 gf. The friction force appeared to increase slightly with increased weight, ranging from 12 to 32 ± 5.5 gf for the aluminum sled and 18 to 50 ±5.5 gf for the copper sled. Friction coefficients were averaged, and determined to be approximately 0.18 and 0.38 for aluminum and copper, respectively.

2.1.1 Summary of existing literature for open bowel specimen friction experiments

For those experiments conducted by pulling with blocks over open specimens, the findings were somewhat inconclusive. X. Wang's group indicated that weight had a negligible effect on the COF [32], whereas Kim's group showed that friction force increased with increasing weight, while the coefficient of friction decreased with increasing weight [30]. It has been suggested that the change in friction coefficient may be affected by the addition of a lubrication layer that is induced when the normal force is increased [30]. The composition of the lubrication layer may consist primarily of saline introduced artificially by the experiment protocol, native secretions that are forced out of the tissue, or a combination of both. It should also be noted that given a relatively similar range of weights, the corresponding friction forces between the three reporting groups were slightly different. For example, Kim and X. Wang's groups both tested weight ranges between approximately 40-340 mN, yet the friction forces reported by X. Wang's group [32] were two to three times that reported by J.S. Kim [30]. The corresponding pressure ranges were relatively similar (80-640 Pa for J.S. Kim and 65-460 Pa for X.Wang) and the velocities also were equivalent. K.D. Wang's results corresponded more closely to those of Kim's, which leads to the suggestion that perhaps material or surface

roughness may have contributed to the results [49]. Kim and K.D. Wang used aluminum and aluminum or copper, respectively [30],[49], while X. Wang's group used ABS plastic [32].

All groups experimenting with velocity tests reported an increase in friction force associated with an increase in velocity. At velocities below 0.5 mm/s, the increases are slight, and may not be significant. With larger increases, it appears that the increase in friction force can attributed to the velocity, however, the increase in resistance force with speed is even more pronounced with increased capsule diameter. J.S. Kim's group noted that "when the capsule speed is lower, the deformation of the intestine wall induced by the capsule generates more slowly and also the stress relaxation of the intestine occurs more during the capsule passage…and leads to lower frictional force [30]." Accoto, *et al* found that force did not depend on velocity during studies performed in the colon [31] while Wang attributed this to different surface tissue features and the reduced mucous substance on the colon compared to small intestine [32].

All of the aforementioned experiments were conducted *in vitro*. Temperature and hydration were taken into account for many of the test setups, but it has not been shown that these is an accurate simulation of *in vivo* conditions. In the majority of the studies, multiple runs were conducted on each tissue sample. The integrity of the mucus layer and underlying tissue over the course of testing was not characterized. Based on these studies, one would expect to see friction forces on the orders of 10^{-1} to 10^{-2} N, with COF on the order of $10^{-1}$to 10^{-3}.

2.2 Closed Specimen Tests

Baek, *et al* evaluated the effect of surface area, edge effects and capsule material inside a closed small intestine specimen [28]. Capsules were pulled at a speed of 0.5 mm/s for three runs through the same specimen sample. When comparing geometry, four aluminum capsule shapes

were used, which included one solid cylindrical capsule and three cylindrical capsules with circumferential cutouts with varying edge effects, ranging from blunt to smoothed. The surface area of the purely cylindrical capsule was 565.5 mm^2 while the surface areas of the corrugated capsules ranged from 743.0 to 645.1 mm^2, in order of sharpest to smoothest leading edge geometry. The results show that the capsule with the most blunt corrugations resulted in higher "startup" friction forces and those three capsules with corrugations had higher friction forces than the cylindrical capsule with no cutouts, by a factor of nearly 2. All three capsules with cutouts had similar average friction forces near 40 mN over the length of travel, while the purely cylindrical capsule averaged friction forces of approximately 20mN. The authors were unable to conclude if the increase in resistance should be attributed to the increase in surface area or the presence of sharp corners which "dig" into the specimen's mucosa. It was suggested that both parameters independently contribute to the increase friction force.

Baek's group also compared friction forces as a function of material, increased capsule diameter and length [28]. Aluminum and acrylic plastic were compared, with diameters ranging from 7 mm to 10 mm and length from 15 mm to 25 mm. No values of material surface roughness were reported. The weights of the aluminum capsules were approximately twice that of the plastic capsules and were related to the changes in capsule dimensions. The aluminum capsules ranged in weight from 21.1 to 44.1 mN while the plastic capsules spanned 9.0 to 18.2 mN. The friction forces on the capsules used in Baek's testing ranged from 20-50 mN. It was initially noted that friction force increased with increased capsule surface area, and the authors also concluded that the force increase was more so a function of diameter increase than for increases in length. The latter result overrode the correlation between increased friction with increased surface area, indicating that minimal enlargements of the diameter contributed to friction forces

more so than increases in contact area. No mention of the correlation between friction force and weight was made. The authors reported that for a unit length increase of 1 mm, the friction force increase was approximately 1.7 mN for aluminum and 1.3 mN for plastic. The increase in friction force per unit increase in diameter was said to be equivalent to that for a 5 mm increase in length, corresponding to approximately 8.5 mN and 6.5 mN for aluminum and plastic, respectively. Baek's group surmised that the contribution to this increase was due primarily to the geometry of the front section of the capsule, which induced greater hoop stresses. They also noted that the friction force varied locally with the morphology and viscoelasticity of the intestine, evidenced by matching peaks and valleys when evaluating measurements of friction forces along the length of each specimen sample [28] .

Kwon, *et al* performed experiments to consider the effects of velocity, diameter, shape, stroke and weight of an object within a closed small intestine specimen [50]. When evaluating velocity effects, a capsule of diameter 13 mm, radius of curvature of 1mm, weight 3.5 gf and stroke of 15 mm was tested over the velocities of 0.2, 0.4, 0.6, 0.8 and 1 mm/s. For each test, the friction force increased with the position of the head along the length of travel. Maximum friction forces between 75-85 gf did not appear to be affected by changes in velocity. It was noted by the authors that the large increases in friction force occurred during the first 3-5 mm of travel as the head and specimen stuck together. Slippage eventually occurred, at which time the tensile force pulling the capsule exceeded that of the friction force between capsule and specimen. The friction force continued to increase, which the author attributed to the "the tensile force of the specimen behind the mobile head (of the capsule) is added on to the slip friction."
In considering diameter effects, diameters of 10, 13 and 15 mm were selected. A radius of curvature was not provided, nor was the speed or material of the capsule given. The maximum

friction force for each of the 10, 13 and 15 mm diameter capsules were 45, 80 and 115 gf, respectively [50]. Kwon's group then considered friction force as a function of radius of the edge of the capsule head. A radius of 1mm yielded a maximum friction force of approximately 75 gf. The radius of 2 mm yielded the lowest maximum force around 35 gf [50]. Finally, Kwon considered the friction force as a function of weight, by varying the weights of the capsules between 2.5 and 3.5 gf. They concluded that the addition of weight in this range had a negligible effect on the friction force between the capsule and the intestinal specimen.

J.S. Kim, in addition to the open specimen experiments listed in Section 2.1, performed closed specimen experiments on capsules of differing diameters being pulled within the specimen at different velocities [30]. The four aluminum capsules were all 20 mm in length, with diameters of 7, 8, 9 and 10 mm. Each had a front and rear radius of curvature of 2 mm, but with differing weights and surface areas. The velocities tested were 0.16, 0.33 and 0.5 mm/s. The group found that friction force increased with increased diameter as well as with increase in velocity. For an increase in velocity of 0.34 mm/s, the increase in friction force for the 7mm capsule ranged from approximately 20 mN to 25 mN, forces for the 8mm capsule increased from 23 mN to 31 mN, for the 9mm capsule the forces increased from 30 mN to 45 mN and for the 10mm capsule the friction forces increased from approximately 46 mN to 58 mN (All values are estimated from a force vs velocity plot. Specific force and uncertainty values were not reported).

Wang's group also studied the friction forces within a closed intestinal specimen. They used capsule shaped geometries of varying dimensions and evaluated the friction force as a function of contact area as well as velocity [32]. They did not evaluate the effect of weight on friction forces during closed specimen experiments, due to the lack of a large enough variation in weight between the plastic capsules. Instead, this evaluation was made on an open specimen, as

noted in Section 2.1. In the closed specimen experiments, five diameters of 8, 9, 10, 11 and 13 mm and three lengths of 20, 23 and 26 mm were selected, and fifteen capsules were fabricated for each of the corresponding combinations. Contact areas ranged from 502.7 mm^2 to 1,061.9 mm^2. The tests were repeated on a total of 6 specimens, with measurements taken every four seconds and a single force value was reported by averaging these measurements. The velocity at which the capsules traveled was 0.5 mm/s. When evaluating friction force as a function of diameter and length, their results show that the force responds more to changes in capsule diameter than to increases in capsule length. For a constant diameter, the force varied within the range of 20 ± 9 mN over changes in length of 6 mm. For a constant length, the resistance force varied by over 60 ± 9 mN for changes in diameter of 5 mm. They took special note of the deviation in resistance force measurements for one specimen sample with a diameter that was notably smaller than the others. The circumferential extension was visually noticeable and resulted in resistance forces that were significantly larger than those measured in the other five samples. Over 95% of resistant force values were in the range of 20-100 mN, with the remaining 5% obtained from smaller diameter specimen.

Wang also evaluated the friction force as a function of velocity, testing velocities of 0.5, 2, 3, 4, 5, 6 and 8 mm/sec. These tests were performed with capsules of length 26mm and diameters ranging from 9 mm to 13 mm, as well as with capsules of a constant diameter of 11 mm with lengths of 20, 23 and 26 mm. It was concluded that resistance force increased with velocity, and the effect was more significant when diameter was increased, which was consistent with results reported for a constant velocity. For a given diameter, the friction force varied by 50 to 80 ± 13 mN for a given speed. For a constant length, the friction force varied by

approximately 20 ± 13 mN. They also noted that friction was “extremely sensitive” to presence of saline.

2.2.1 Summary of literature reporting results for closed bowel specimen friction experiments

In closed experiments that evaluated friction forces on the basis of weight, the conclusion was that the effect of weight was negligible. The weights tested for these experiments were less than 50 mN, and changes in weight were typically associated with changes in capsule dimension.

A number of groups hypothesized that increased contact area of a capsule would have a positive correlation to friction force. The hypothesis was not disproven, as capsules with larger surface areas registered larger forces, however upon further dissection, each group independently concluded that the increase in force was in large part due to the capsule’s diameter and geometry. Baek, *et al* noted that a one unit increase in capsule diameter yielded equivalent friction forces to that when length was increased by five units [28]. This increase was despite the length increase producing a surfaces area nearly twice as large as that for the diameter increase. However, based on the results of the corrugated capsule experiment, Baek suggested that contact area does have some contribution to resistance forces, albeit undetermined. They noted that the friction forces for the capsules with corrugations was about two times higher than the capsule with a smooth cylindrical shape, while the differences in surface area were between 15-30%. It is also important to note that the measured surface area was not necessarily equal to the real contact area between the capsule and specimen. However, because of the nature of the intestinal specimen’s compliance, Baek noted, “it can be assumed that the real contact area will increase with the increase in the apparent surface area of the capsule [28].” They conceded only that the “increase in frictional resistance of the capsule with corrugations depends on the increase in the contact

area...in addition to the effect of the capsule corners." This conclusion is similar to one that many others have made, however, at this time there is no literature that reports experimental data related to the effects of the leading edge geometry on the resistance force.

2.3 Conclusions

Making quantitative conclusions from based on the total research findings of the above authors can prove to be difficult, as the methods, conditions and sliding specimens used by each research group varied so greatly. However, it is possible to derive qualitative conclusions and estimate a range of frictions forces that the capsule can reasonably expect to encounter, based on the chosen geometry, dimensions and velocity. In addition to differences in force measurements and friction coefficients recorded between research groups, there were also large differences in the forces reported from the same group when considering the friction forces recorded for sleds of the same size, dimension, weight and velocity for tests evaluating different parameters.

Above all, it is evident that the small intestine is a complex organ with highly variable surface properties. Its viscoelastic properties play an integral role in its friction response to a number of parameters, many of which appear to be interdependent. Geometry, edge effects and velocity are those parameters with the largest contributions to changes in friction forces, which imply that a dry friction model may have error associated with it. Additionally, future experimental data collection should be obtained while the intestinal specimen is in nearly its natural state. Specimen hydration may also affect results.

In this work, the friction response of the small bowel lumen surface was measured when a coupon of varying speed, pressure, material and contact area was passed upon it. The hypothesis, formed following a thorough literature review, predicted that the COF would increase non-linearly with increases in velocity and linearly with pressure and contact area. We

predicted that PDMS would yield the highest COF of the engineering materials tested, followed by stainless steel and polycarbonate, respectively.

Chapter 3

Methods

A comprehensive, iterative process of evaluating the friction force between the small bowel lumen surface and various engineering materials was executed using a tribometer. The testing parameters were selected to compare and expand upon the results reported in Chapter 2. A preliminary goal was to capture friction measurements *in situ* and compare those to data collected *in vitro* to verify that *in vitro* testing conditions were an accurate representation of the true measurements. Variables such as velocity, pressure, contact area and material were integrated following early testing observations. As a result, both the experimental design and testing equipment design evolved significantly over the span of this research project. The following sections describe the tribometer design(s), ad hoc testing observations and subsequent alterations that were made to address the testing observations.

3.1 Initial Tribometer Design: Curved Sled with Edge Effects

The first tribometer was designed prior to having any physical interaction with intestinal tissue. A Solidworks assembly of the initial design is shown in Figure 4. The initial tribometer was comprised of a linear actuator which moved a load cell along a linear slide, with the load cell pulling a cylindrical polycarbonate sled along the intestinal specimen seated within a curved tray. A motor driver, data acquisition system and bridge strain measurement module controlled the motion of the sled and recorded position, time, and force. The sled was attached to the load

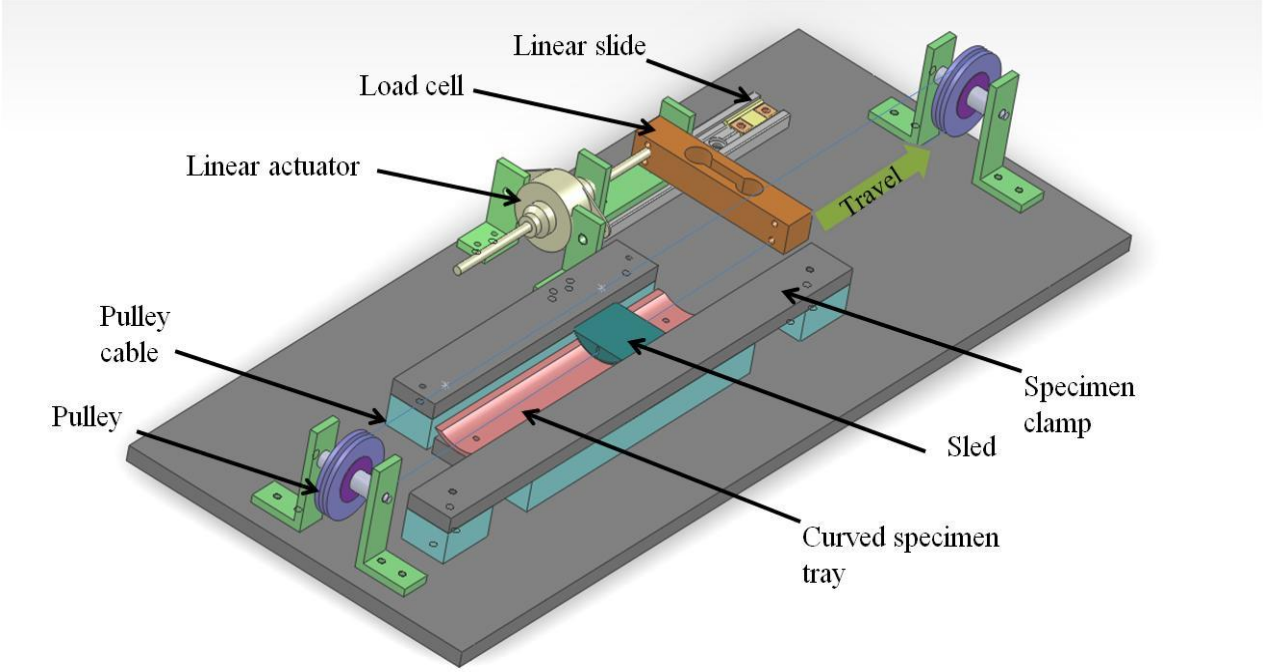

Figure 4. Preliminary tribometer design with pulleys and curved polycarbonate sled

cell by a polymer string. Two pulleys were initially mounted fore and aft of the load cell and tissue specimen in order to maintain sled alignment within the specimen tray, but were removed during testing, along with the specimen clamps, as they were deemed unnecessary.

A curved specimen tray design was conceived with the intent to position the splayed tissue so that the flaccid intestinal villi were positioned radially inward, similar to their orientation *in vivo* when a food bolus, or in this case, an endoscopic capsule, is present. The specimen tray formed a 60° arc with diameter of 3.5 cm, the latter of which was designed to equate to the outer diameter of the small bowel. A specimen with diameter and wall thickness of 3 to 4 cm and 1 mm, respectively was assumed based on the average measurements observed in the small bowel [17],[51]. The cylindrical polycarbonate sled was machined with a diameter of

3.1 cm so as to lie concentrically within the tissue specimen and tray. The leading edge of the sled was machined to a radius of curvature of 1.9 mm.

3.1.1 Materials and Fabrication

Solidworks was used to model the machine's conceptual design, which aided in scaling of the materials as well as alignment of the sled, load cell, motor and linear slide. Part drawings were then produced for use in machining, with tolerances averaging ± 0.1 inch. A Bill of Materials and part drawings are included in Appendix A and B respectively. Aluminum was used for the specimen tray, tray lift, actuator mounts, the load cell carriage and the base plate. The parts were machined with use of a mill, lathe, bandsaw and drill press. The sleds were fabricated from polycarbonate and hand sanded with 800 grit sandpaper. An image of the fabricated machine is shown in Figure 5.

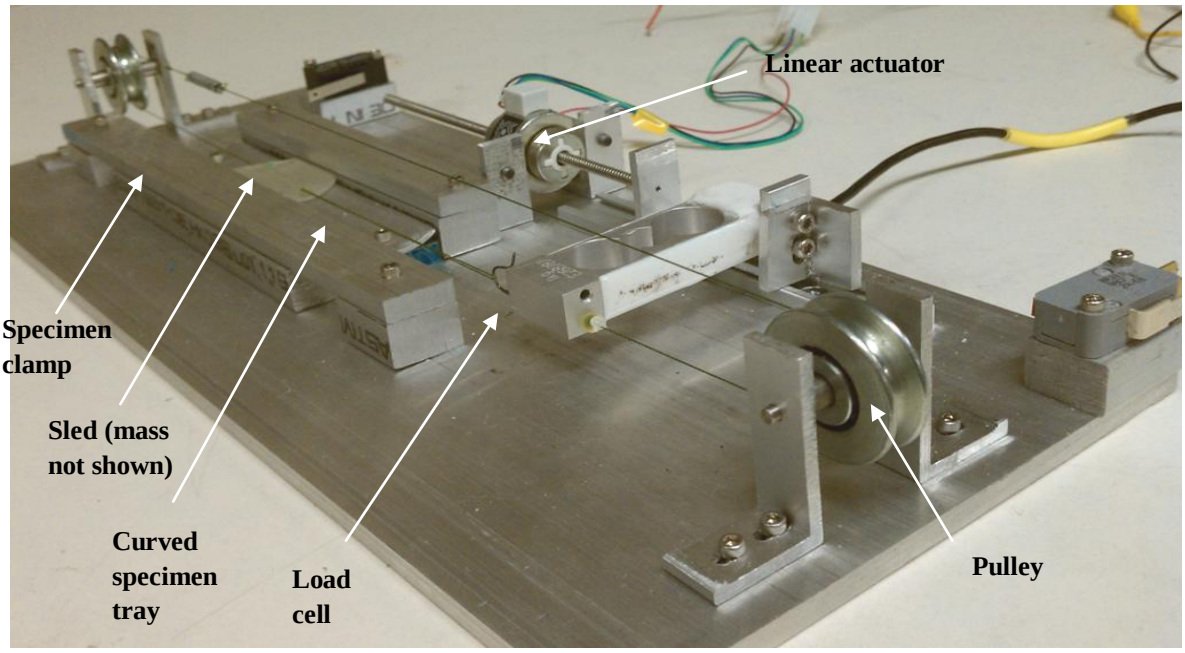

Figure 5. Preliminary tribometer design used for measuring shear friction forces between a curved polycarbonate sled and porcine small bowel lumen (pulleys later removed).

3.1.2 Electronics and Measurement

Motor Speed and Direction Control

A linear stepper motor was selected to drive the load cell and sled system, which provided the ability to control the speed at which the sled was pulled across the intestinal specimen. LabVIEW programming controlled the speed and direction of the motor based on input from the user. The motor driver sent voltage pulses to the motor, controlling the frequency at which the motor took "steps" and drove the actuating mechanism (lead screw) forward. By altering the frequency of these steps, the motor speed could be increased or decreased. A schematic of the hardware and equipment setup is shown in Figure 6.

An electronic switch system was also implemented, which indicated when the load cell carriage, and thus the sled, reached the end of its travel distance. Once a switch was triggered, motor movement as well as load cell measurement ceased. Two switches were located at either end of the motor/linear slide system and when contact was made with the switch button by either the load cell carriage or the actuator's lead screw (depending on whether the system was moving forward or in reverse), the software programming cycle sent signals to the motor driver to abort.

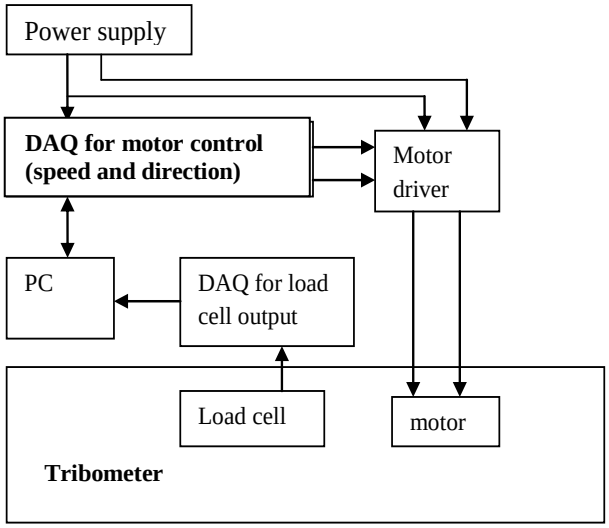

Figure 6. Schematic of tribometer force measurement system for *in vitro* testing

Force Data Acquisition

To capture force measurements of the shear interactions between the tribometer sled and the tissue lumen, a one-kilogram (kg) capacity load cell was used. As the sled was pulled across the specimen, it exhibited a cantilever beam-like deflection upon the load cell. The load

cell, with an internal strain gauge, registered a voltage difference across its internal resistor bridge, which was sent to the data acquisition device and recorded using LabVIEW software.

An excitation voltage of five volts was applied to the load cell, which corresponded to an output range of ± 6.405 mV. Once the voltage signal was received, it was converted to a force measurement. This was calculated by considering a linear relationship between voltage and force and solving for the slope, *m*:

$$y = mx + b \tag{3}$$

LabVIEW programming was utilized to offset the intercept, *b*, to equal zero at the start of each run. The variable *x* is considered to be the voltage output from the load cell and the *y*-term is the corresponding force on the load cell. Using the calibration data from the load cell manufacturer, when a mass of 1kg was applied, the full scale output is 1.281 mV/V. However, after performing a calibration study, the output ratio was adjusted to 1.128 mV/V to yield a conversion factor of 1,739 N/mV when applying 5 volts of excitation to the strain gauge. The load cell was calibrated by adding incremental weights and measuring the voltage output from the load cell. The weights and the corresponding load cell voltage were plotted, and a regression analysis yielded an R-squared value of 0.999. The calibration data and corresponding calculations are included in Appendix C. The conversion value of 1,739 N/mV was built into the software to output a force reading along with the corresponding time, which was written to a spreadsheet for data analysis.

Data samples of the load cell voltage output were collected at a frequency of 1,000 samples per second. The friction force samples for each run over a tissue specimen were averaged over the length of travel to form one data point for each run. 95% confidence intervals

were then calculated to estimate a population mean with these sample means. The sample means were compared using an Analysis of Variance (ANOVA) test, assuming equal but unknown variances. Sample sizes for each study were selected with the intent to produce the greatest possible sensitivity based on tissue availability. Friction forces and coefficients are reported in the results section.

3.1.3 *In situ* vs. *In vitro* Comparison (Curved Sled)

For the initial round of testing, the research goal was to determine if a difference existed between the measured friction forces on tissue in its *in situ* state as compared to tissue which had been extracted from the animal, stored in a 0.9% PBS solution and later prepared *in vitro*. *In situ* tests were performed on an anesthetized porcine model (IACUC protocol 87909(05)1D, Ref#100587). Porcine intestinal tissue has been shown to be similar to humans in both its physical and physiological characteristics [38],[51],[52]. In order to reduce the amount of food debris in the gastrointestinal tract, the animal was placed on a Jell-O diet starting 48 hours prior to surgery, replaced by a Gatorade-only diet for the final 24 hours preceding surgery. The tests were performed by extracting a section of small bowel from a porcine abdomen and cutting open along the longitudinal axis near the mesentery. With the mesentery intact, the specimen was brought to the tribometer and splayed upon the curved specimen tray.

For the test, the curved polycarbonate sled with contact area 6.97 cm^2 was loaded with a mass of 50 grams in order to simulate an average intra-abdominal pressure of 760 Pa (5.7 mmHg) [20] and pulled across the tissue specimen at a linear velocity of 1 mm/sec. Each treatment combination was repeated three times on each of two pieces of tissue yielding six data points for each section of bowel, with the exception of the middle section. Tests were not conducted on this section due to constraints on surgery time.

Following *in situ* testing, the intestinal tissue from the test was harvested and stored in PBS solution at 3 °C for approximately two hours and was then brought to room temperature (20°C) for testing. The tests conducted *in situ* were repeated on adjacent tissue specimens *in vitro* within five hours of tissue excision. The sled weight, tissue contact area and velocity were held constant for both tests. During the tests, the mucosa was kept hydrated by applying PBS to the tissue surface using a syringe dropper. Six data points were again collected for each of the three sections of the bowel. A summary table of the testing variables is provided in Table 1.

Table 1. Testing parameters for tribometer with curved sled

Testing Factor	Testing level(s)
Tissue state	*In situ, in vitro*
Region	Proximal, Middle, Distal
Sled geometry	Cylindrical
Sled material	Machined polycarbonate
Sled weight	0.53 N
Sled contact area	6.97 cm^2
Sled pressure	0.76 kPa
Sled velocity	1 mm/s

An abridged follow-up study was conducted to compare the curved sled and specimen tray with a flat polycarbonate sled which traveled upon a flat tissue specimen. The weight, material, velocity and contact area of both sleds were equal to the previous study. The intent of this study to was to evaluate if tissue positioning affected the friction response of the tissue to a measureable degree. Three runs on two tissue samples from the proximal small bowel were conducted for each configuration. The results are provided in Chapter 4.

3.2 Tribometer Re-design: Sled with Negligible Edge Effects

While performing tests with the curved sled, mucus was observed building up at the leading edge of the sled as the sled moved along its length of travel. Upon inspection of force vs. sled displacement plots from the data collected during each run on the tissue, it appeared that the measured friction force was increasing as the sled moved along the tissue surface. This suggested that the mucus build-up at the front face of the moving sled was inducing an additional fluid drag force concurrent with the friction force being measured. It is well known that velocity, v, edge effects arising from geometry, C_d, and the cross-sectional area of a of a vessel, A, moving through a fluid with density ρ, influence the fluid drag within a viscous fluid, according to (4) [53],[54]:

$$\text{Force}_{drag} = \frac{1}{2}\rho v^2 C_d A \qquad (4)$$

In order to minimize contributions from fluid drag and to "normalize" the surface interaction effects between the leading edge of the sled and the tissue surface, the curved sled was replaced with a flat, overhanging "edgeless" sled. The sled in translation was designed to extend beyond the raised area of the splayed intestinal specimen on all sides, with the intent of eliminating effects from sled edge--tissue interactions. Polished stainless steel was selected for the sled material so as to reduce surface roughness to the extent that the primary mechanisms of friction could be reduced to a combination of adhesion and fluid shear, rather than to deformations of asperities on the material surface. With no discontinuities between the sled surface in contact with the tissue, it was hypothesized that fluid drag effects would be minimized and the force measurements being collected would be indicative of the "pure" sliding friction forces between the sled material and the tissue lumen. The curved specimen tray was replaced

with a flat tissue tray for this study. A bill of materials and part drawings (for those in addition to the initial tribometer design) for this machine are provided in Appendix D and E. A schematic of the overhanging sled and the revised tribometer before and during *in situ* testing, respectively, are shown below in Figure 7, Figure 8, and Figure 9.

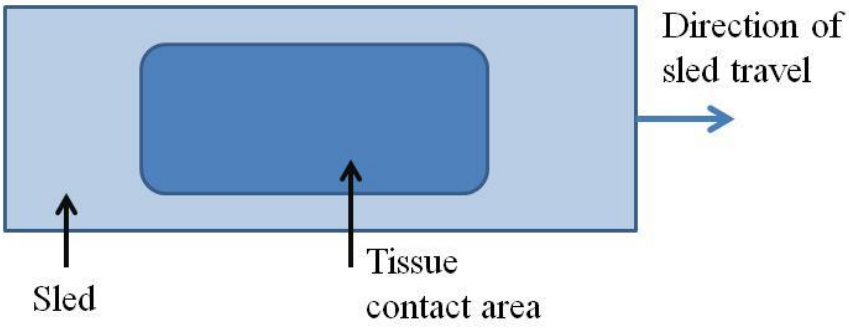

Figure 7. Schematic of overhanging sled above open small bowel tissue specimen, yielding negligible edge effects

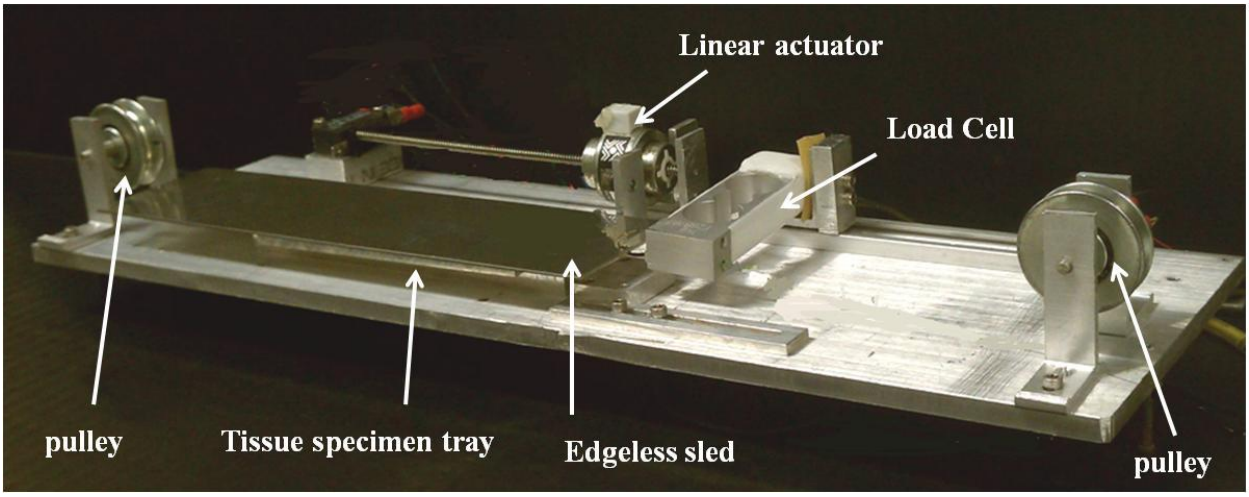

Figure 8. Tribometer design with edgeless sled

3.2.1 *In situ* vs. *In vitro* Testing

Initial *in situ* and *in vitro* testing was conducted using the original tribometer, with sled modifications noted above and a mounted pulley system. Two pulleys were mounted fore and aft

of the overhanging sled and served to align the central axis of the sled over the tissue specimen. The polymer string connected the front of the sled to the load cell and passed through the front and rear pulleys before re-attaching to the trailing end of the sled. A spring (with known constant) was positioned in series with the cable line to provide tension. As the load cell was driven forward by the linear actuator, the weighted sled was pulled over the fixed intestinal specimen while the pulley and cable system maintained alignment with the line of action of the load cell.

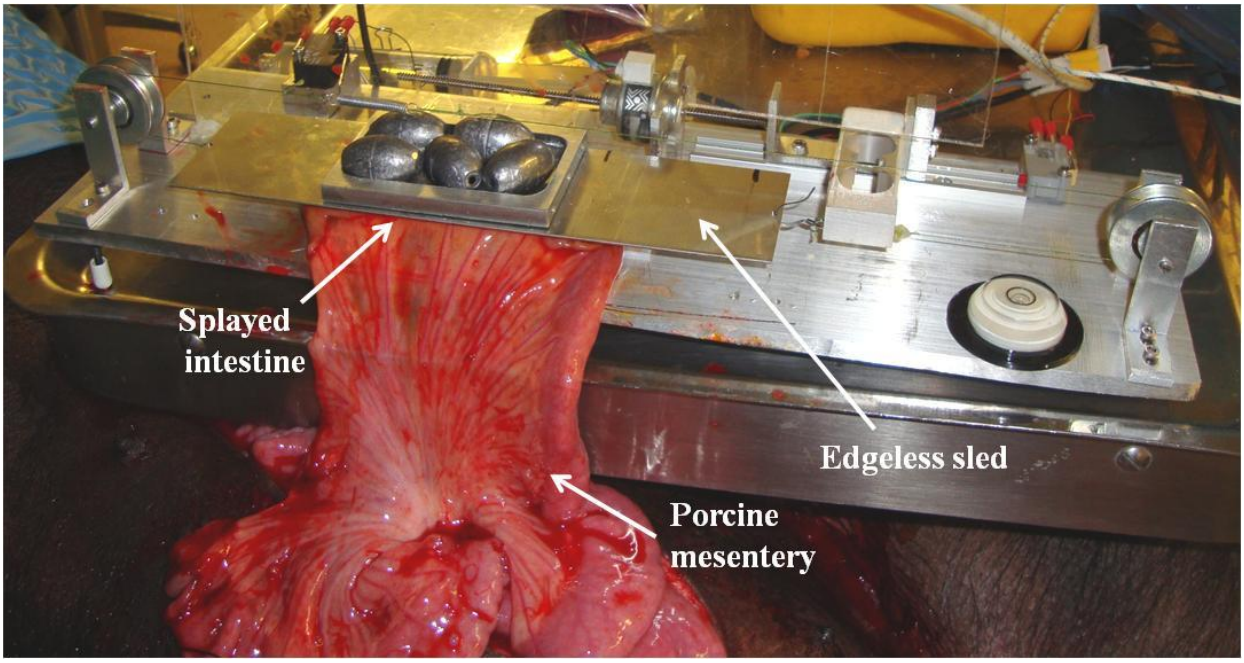

Figure 9. Tribometer with edgeless sled during *in situ* testing

The *in situ* tests were performed as in Section 3.1.3 by extracting a section of small bowel from a porcine abdomen and cutting open along the longitudinal axis near the mesentery. With the mesentery intact, the specimen was brought to the tribometer and splayed upon a raised specimen tray with contact area 38.7 cm^2. The tissue was affixed to metal barbs which protruded orthogonally from the vertical sides of the specimen tray. The sled was weighted with 3.21 N.

The tray contact area and sled weight were again selected so as to approximate the body's intra-abdominal pressure, in this case 0.83 kPa (6.2 mmHg) [20]. *In situ* testing was conducted on two tissue samples from each of three regions (proximal, middle and distal) of the small bowel. Three runs were performed on each specimen sample at a velocity of 1 mm/s.

The above mentioned tests were then repeated *in vitro.* With regards to tissue handling, the aforementioned protocol from section 3.1.3 was followed. Six data point from each region of the bowel were collected for the *in vitro* tests.

3.2.2 Pressure test

Six pressure levels were tested by adjusting sled weight over a range of three different contact areas. The weights were varied between 1.16 and 3.21N and the contact areas ranged between19 and 39 cm^2. The pressures ranged from 0.3 to 1.7 kPa. This pressure range was selected to correspond to the pressure reported in other bowel friction measurement studies as well as to pressures that may represent the resultant pressure of the contractile muscle response from the bowel wall in response to a bolus [28],[30],[32]. Three runs on each section of the bowel were conducted, forming three data points per region.

3.2.3 Velocity test

The translation speed of the sled moving across the tissue surface was also evaluated *in vitro* with this tribometer design. For the velocity testing, a 0.94 N weighted sled was pulled across a tissue surface with approximate contact area of 39 cm^2 at speeds of 0.5, 1, 2, 4 and 6 mm/s. The pressure for this study was chosen to more closely match pressures indicated from other studies [28],[30],[32] so as to evaluate the significance of eliminating the sled edge. Each velocity was evaluated on three tissue samples from three regions of the small bowel (proximal,

middle and distal regions), for a total of six samples for each region. Table 2 summarizes the testing parameters.

Table 2. Testing factors and associated levels for tribometry experiment with edgeless sled

Testing Factor	Testing level(s)
Tissue state	*In situ, in vitro*
Region	Proximal, Middle, Distal
Sled geometry	Edgeless
Sled material	Stainless steel
Sled weight	1.16 N, 3.21 N
Sled contact area	19 - 39cm^2 (3 levels)
Sled pressure	0.3 - 1.7 kPa (6 levels)
Sled velocity	0.5 - 6 mm/s (5 levels)

3.2.4 Verification test

After analyzing the friction behavior along the length of travel for each run using the overhanging sled tribometer, topography fluctuations were not detected. In order to determine if this was due to the elimination of sled edge effects, the increased sled pressure or a consequence of pulley noise, the pulleys were removed and a subset of the above described *in vitro* tests were conducted. Care was taken to precisely place the sled so its center of mass was directly over the tissue specimen. A schematic of this setup is shown in Figure 10.

As with the velocity experiment, a 0.94 N weighted sled was pulled across a tissue surface with approximate contact area of 38.7 cm^2. A verification comparison was made by measuring the mean friction force for a sled translating at speeds of 0.5 and 6 mm/s. Force measurements and subsequent data analysis were obtained and processed as described above.

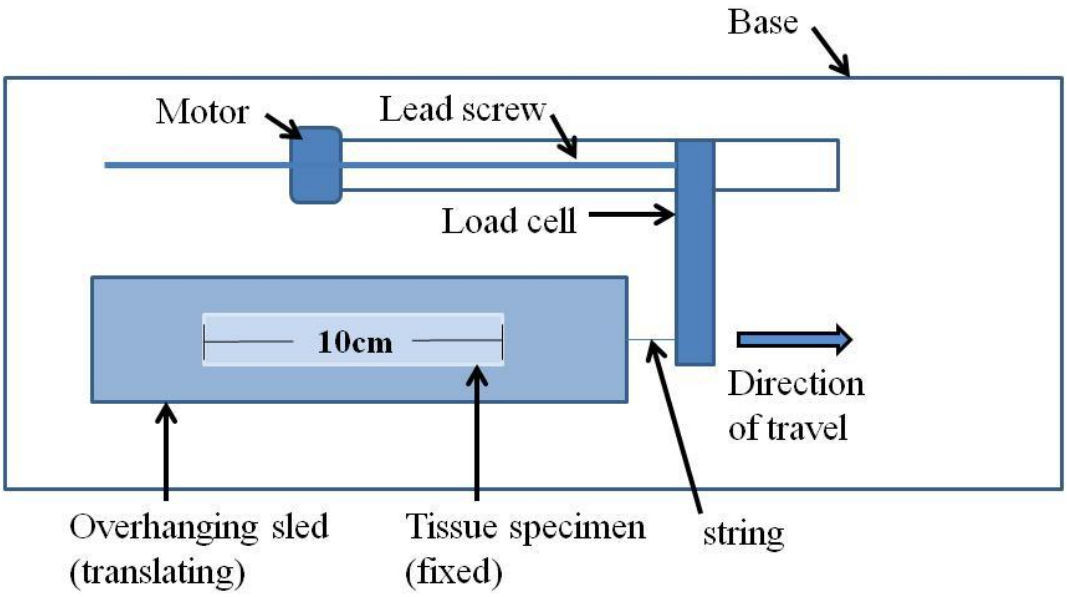

Figure 10. Schematic of tribometer setup with pure sliding where the overhanging sled translates across the surface of a fixed, splayed small bowel tissue specimen.

3.3 Final Tribometer Design: Sled with Negligible Edge Effects

The tribometer was modified once more in order to eliminate sled stabilization effects. Because of the low friction between the sled and the intestinal tissue, the overhanging sled required precise alignment with the load cell's line of action. In order to eliminate the measurement noise produced by the pulleys and to simplify the design, the sled and testing surface were inverted. For this design, the testing material (formerly the overhanging sled) was fixed to the tribometer base and served as a flat surface, while the tissue specimen was clamped into a fixture with a protrusion of prescribed contact area and translated horizontally up the testing material, which is shown in Figure 11. The bill of materials for the final tribometer design and Solidworks drawings for the tissue fixtures are shown in Appendix F and G, respectively, and an image of the final tribometer design being used for testing is shown in Figure 12.

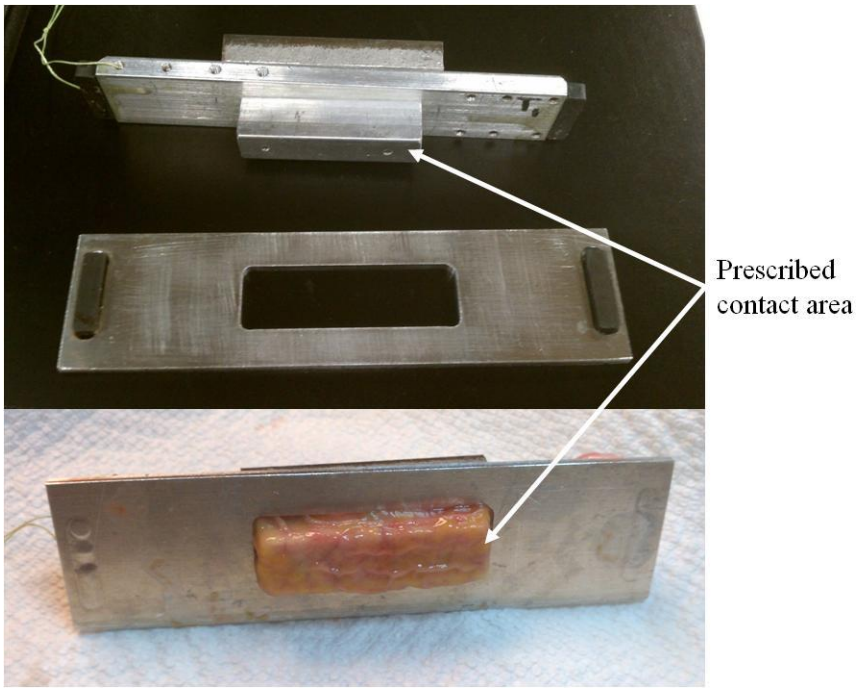

Figure 11. Tissue clamping fixtures for use with final tribometer design

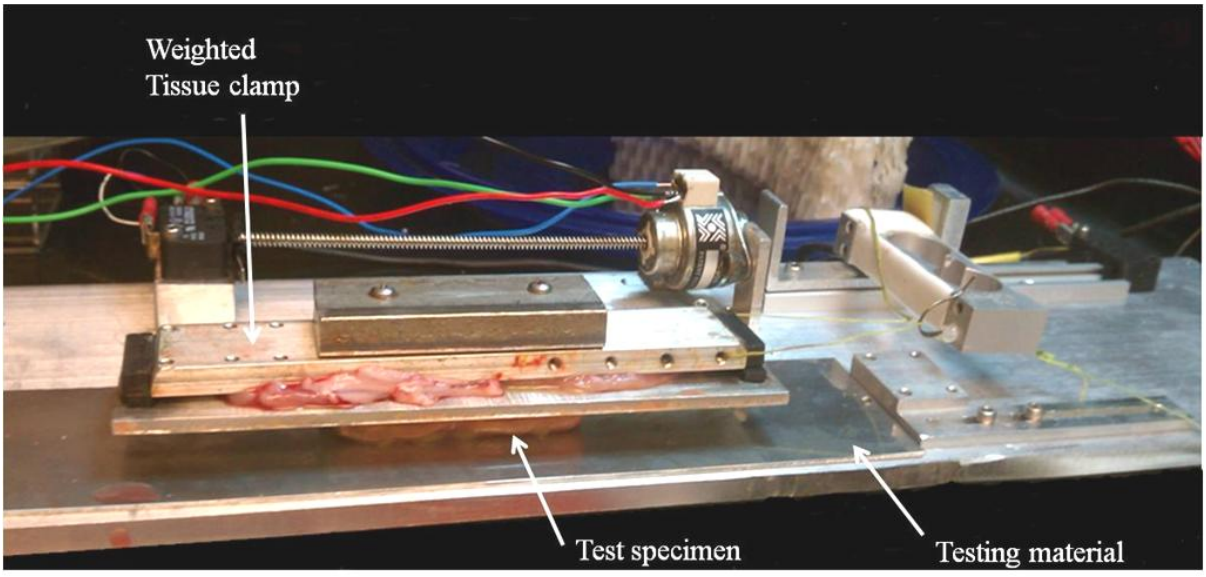

Figure 12. Final tribometer during testing

During previous testing, tissue drying was observed and remedied by applying saline to the tissue surface. However, speculations remained that the saline may have adverse outcomes on the friction measurements. In order to more closely approximate the climate *in vivo*, an environmental control chamber was designed. The environmental control chamber was designed

with the ability to add heat and humidity to a closed system, within which the tribometry experiments were conducted. The control chamber housed the tribometer and associated data collection equipment, three heaters and water reservoirs. The heaters were mounted on three of the vertical walls and the water reservoirs were placed directly underneath. The heaters consisted of Nichrome wire wrapped around an electrically insulated frame to which a small PC fan was mounted. Electrical current input to the Nichrome wire was controlled so that the temperature within the chamber was held to 37.5 ± 0.5 °C. Voltage control over the heater fans (passing warm air over the water reservoirs) maintained 95 ± 3 % relative humidity within the chamber. A Solidworks model of the control chamber can be seen in Figure 13.

In order to optimize the experiment in terms of time, tissue allocation and other laboratory resources, a designed experiment was executed. A fully-crossed, mixed effects (Type III) model was deemed appropriate based on the selected testing factors. To evaluate the variability attributed to the animal population from which the tissue was extracted, pig was identified as a random variable. Bowel region, sled material and sled contact area were three additional factors evaluated for the final study, identified as fixed factors. The measured variables, their corresponding levels and effect type are listed below in Table 3.

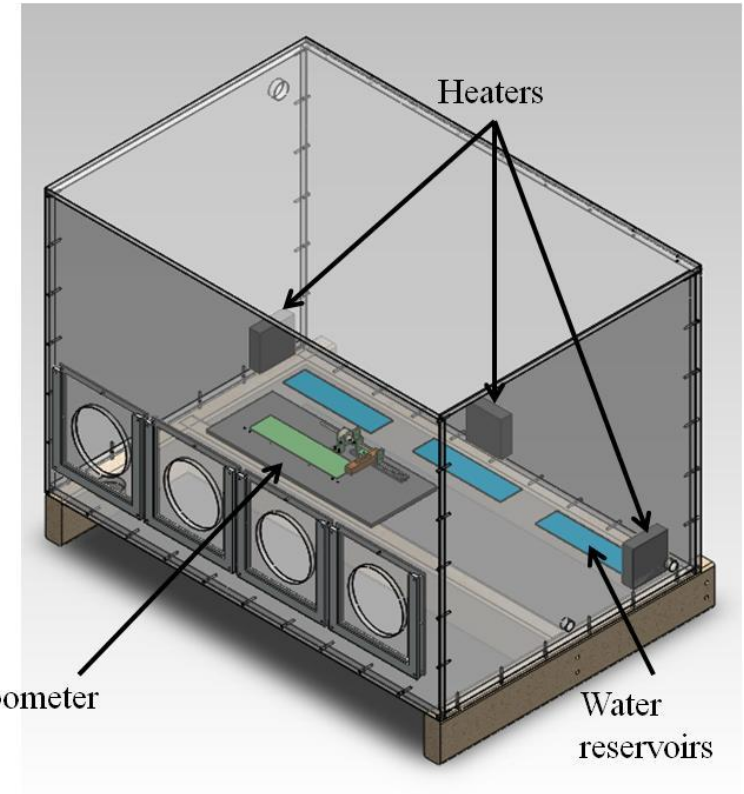

Figure 13. Solidworks model depicting tribometer within environmental control chamber for final experiment

Table 3. Testing Factors and associated levels for final tribometry experiment

Testing Factor	Testing level(s)
Pig	Random (3)
Tissue state	*In vitro*
Region	Fixed: Proximal, Middle, Distal
Sled geometry	Edgeless
Sled material	Fixed: Stainless steel, polycarbonate, PDMS
Sled weight	2.3 N, 4.7 N
Sled contact area	Fixed: 6.5 cm^2, 12.9 cm^2
Sled pressure	3.6 kPa
Sled velocity	6 mm/s

The bowel was divided into three regions, as in the previous studies. Three sled materials were chosen which represent viable engineering materials which could be considered for capsule

materials. Stainless steel and polycarbonate are two biocompatible materials being considered for body material. The third material, Polydimethylsiloxane (PDMS), was tested to quantify the magnitude of the hypothesized increase in friction over the two body materials. PDMS with columnar pillars has been shown to provide increased friction resistance when compared to smooth PDMS or other engineering materials [39]. For this reason, micro-patterned PDMS is being evaluated as a potential tread for the rotating belts used for capsule actuation [15],[55][56]. Finally, contact area was evaluated by using tissue fixtures with two different protruding contact areas. The larger of the two contact areas was 1290 mm^2 which was approximately equal to that of the existing pill cam. The smaller contact area was 650 mm^2 in order to closely match the surface area of the cylindrical bolus (690 mm^2) from which bowel contractile forces were measured in [26]. (It should be noted that the radius of the bolus likely contributed to an increased stress response from the passive tissue response, however this was normalized from the contractile force measurements.) From the aforementioned study, forces ranging from 1.2 N to 5.7 N per cm^2 were measured, yielding a median pressure of 3.6 kPa. In the final experiment the weight of the sled was adjusted to maintain a constant pressure of 3.6 kPa.

For this experiment, each treatment combination was tested two times, for a total of 81 runs over the lengths of the proximal, middle and distal small bowel. This was repeated for three animals. In order to determine if the main effects or their interactions had a significant impact on the mean friction values, a 4-way ANOVA was conducted. A significance level of alpha = 0.05 and p-value of 0.05 were identified. The results are provided in Chapter 4.

Chapter 4

Experimental Results

The data from each experiment was collected and analyzed as described in Chapter 3. The following section highlights the results from these experiments. Statistical methods are described for each suite of experiments.

4.1 Initial Tribometer Design: Curved Sled with Edge Effects

4.1.1. *In situ* vs. *in vitro* Results

The results of the *in situ* vs. *in vitro* comparison test described in Section 3.1.3 are shown in Figure 14. Each data point was formed by taking the average friction force over six runs (three runs each on two tissue samples) on each section of the bowel. A friction coefficient was then extracted by solving for μ, seen in Equation (2), and plotted for the proximal, middle and distal section of the bowel. The error bars on the plot represent a 95% confidence interval on the mean. The average COF's are 0.015 ± .0.003 and 0.019 ± 0.006, for *in situ* and *in vitro*, respectively. An ANOVA indicated no statistically significant difference between *in situ* versus *in vitro* testing conditions, nor bowel region. The analysis was performed allowing for a 5% probability of making a Type I statistical error ($p = 0.05$).

During testing, particularly for those runs performed *in vitro*, mucus was observed building up at the leading edge of the sled. This is highlighted in Figure 15. Additionally, the measured friction force was higher for the first run across each new tissue sample when

compared to subsequent runs on the same piece of tissue. A plot of the friction force as a function of sled displacement is shown in Figure 16 which illustrates this as well as the presence of localized surface topography.

The results of the evaluation of the curved sled and specimen tray and the flat configuration indicate no statistically significant difference in COF. The comparison is shown in Figure 17. The average COF over 6 runs on proximal bowel tissue were 0.017 ± 0.004 and 0.015 ± 0.002, respectively.

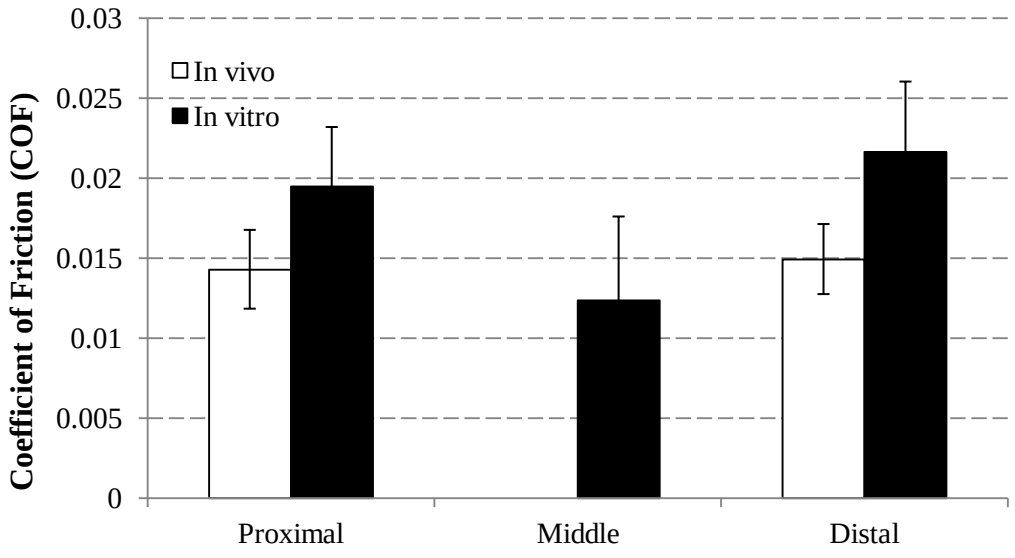

Figure 14. COF of machined polycarbonate on small bowel mucosa. Error bars represent a 95% confidence interval around the mean.

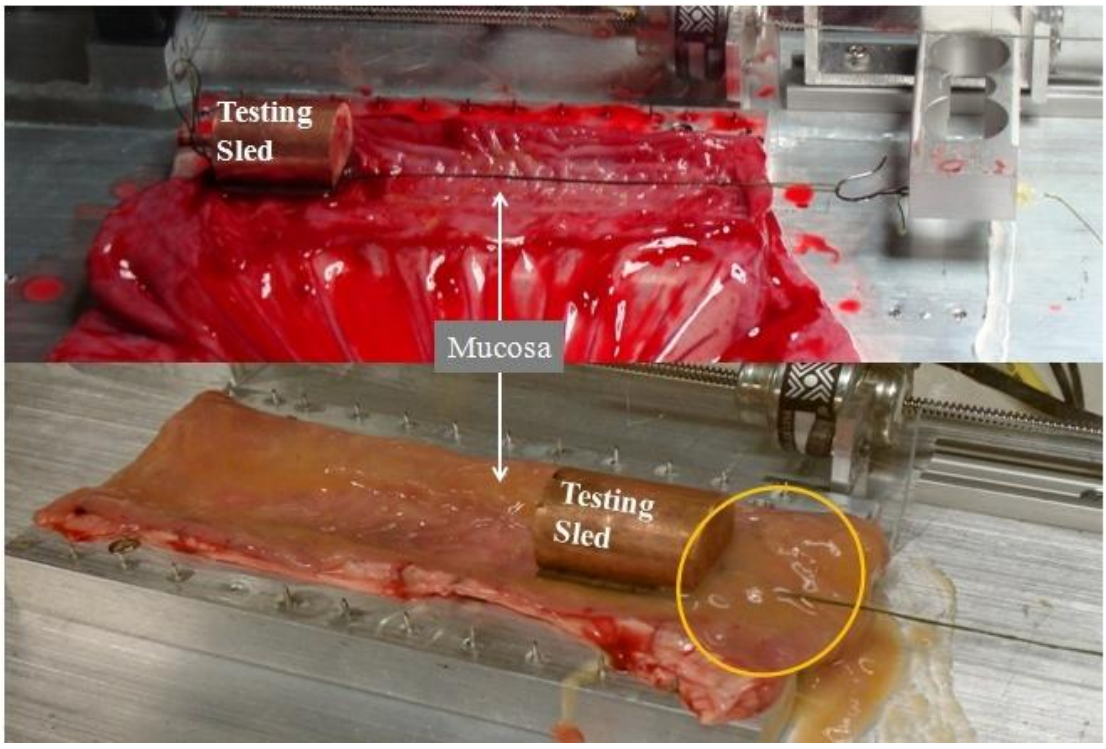

Figure 15. Curved polycarbonate sled during translation across small bowel mucosa during *in situ* (top) and *in vitro* (bottom) testing. Mucus build-up can be seen at the leading edge of the sled during *in vitro* testing.

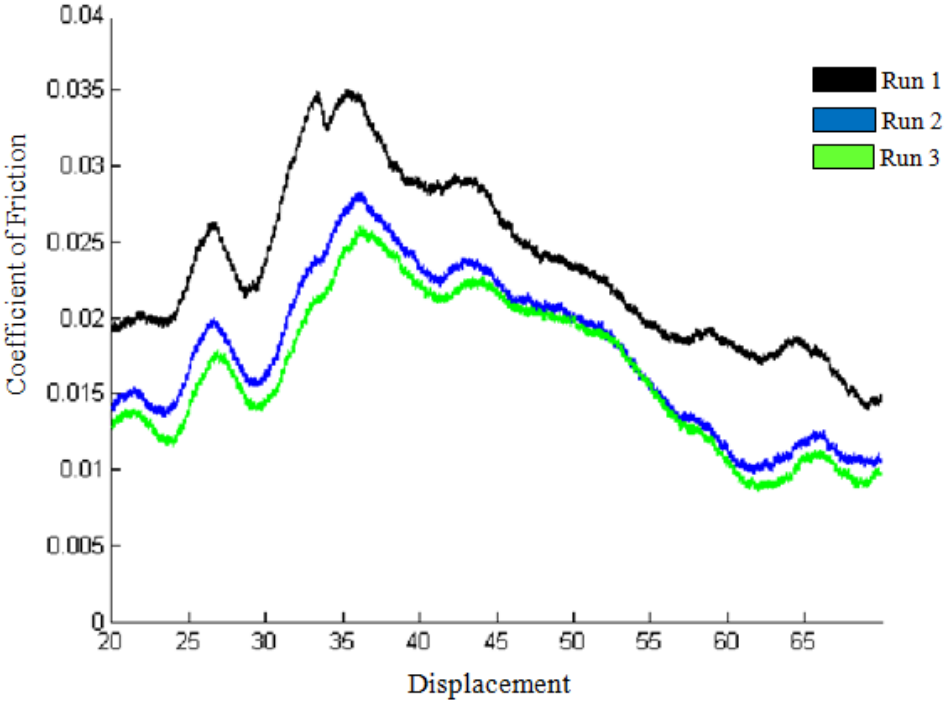

Figure 16. COF vs. displacement for three runs on small bowel porcine tissue (curved sled)

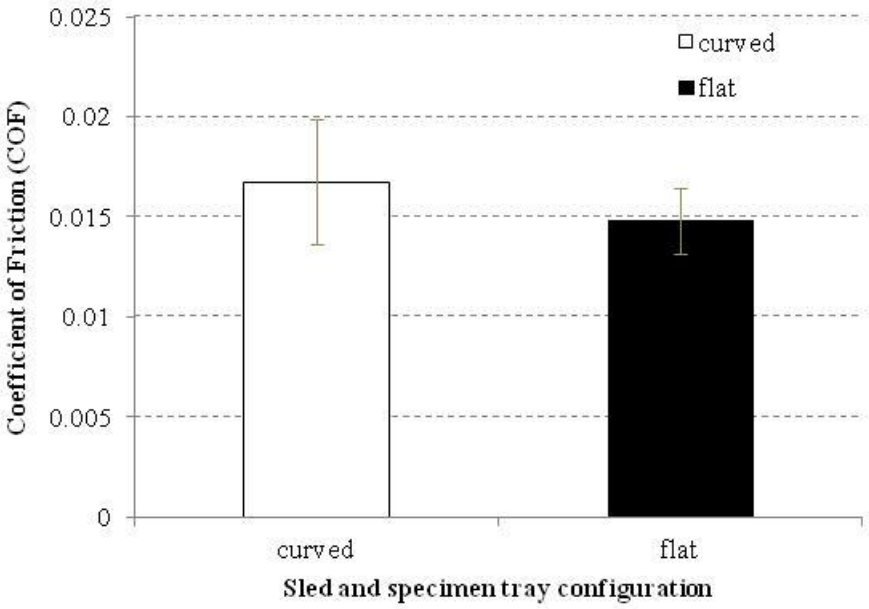

Figure 17. COF for curved specimen tray and sled as compared to a flat specimen tray and sled. Error bars indicate a 95% confidence interval on the mean.

4.2 Tribometer Redesign: Sled with Negligible Edge Effects

4.2.1 *In situ* vs. *in vitro* Results

The friction force values from the *in situ* tests and *in vitro* tests outlined in Section 3.2.1 are shown in Figure 18. These results represent the mean friction force along with the 95% confidence interval for the referenced bowel location and testing conditions. The average COF's are 0.010 ±.0.002 and 0.012 ± 0.002, for *in situ* and *in vitro*, respectively. The temperature of the specimen surface was recorded throughout the course of testing, and ranged from 24.2 to 28.5 ºC for *in situ* tests and 19.1 to 21.4 ºC for *in vitro* tests.

A two-factor ANOVA showed strong evidence that the mean friction values of the *in situ* and *in vitro* tissue samples were different in the proximal and distal sections (p = 0.003, p = 0.01), while the null hypothesis could not be rejected in the middle section (p = 0.053, $F < F_{crit,}$). The analysis was performed allowing for a 5% probability of making a Type I statistical error.

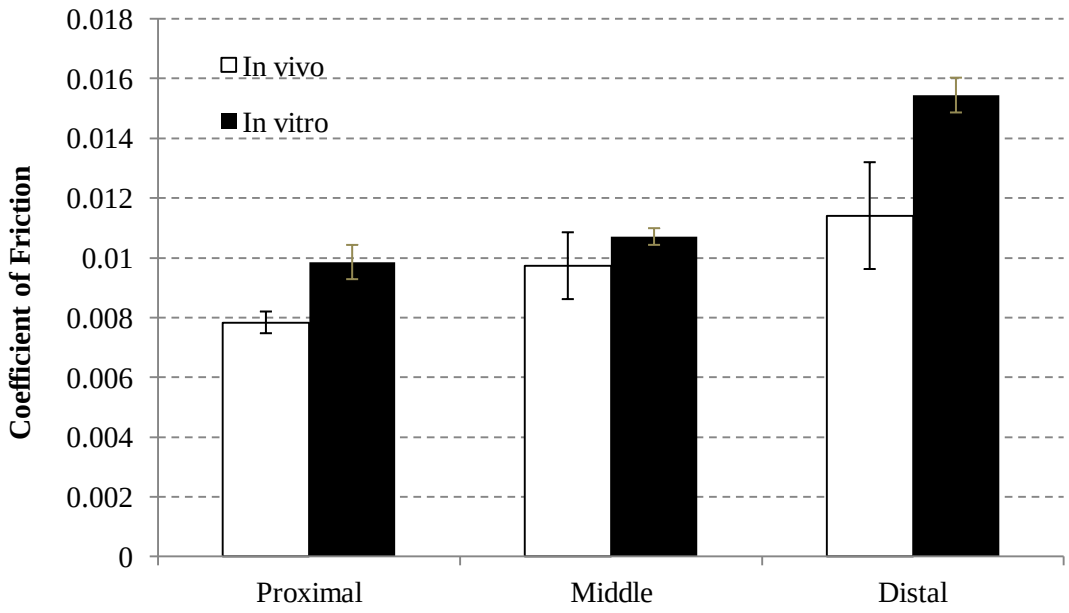

Figure 18. Coefficient of Friction for 3.21 N edgeless, polished stainless steel sled on small bowel mucosa; *in situ* vs. *in vitro* results. Error bars represent a 95% confidence interval around the mean.

4.2.2 Pressure Results

The COF values measured for each pressure-region combination are shown in Figure 19. A 2-way ANOVA indicated no statistically significant difference in COF with pressure, nor between middle and proximal bowel.

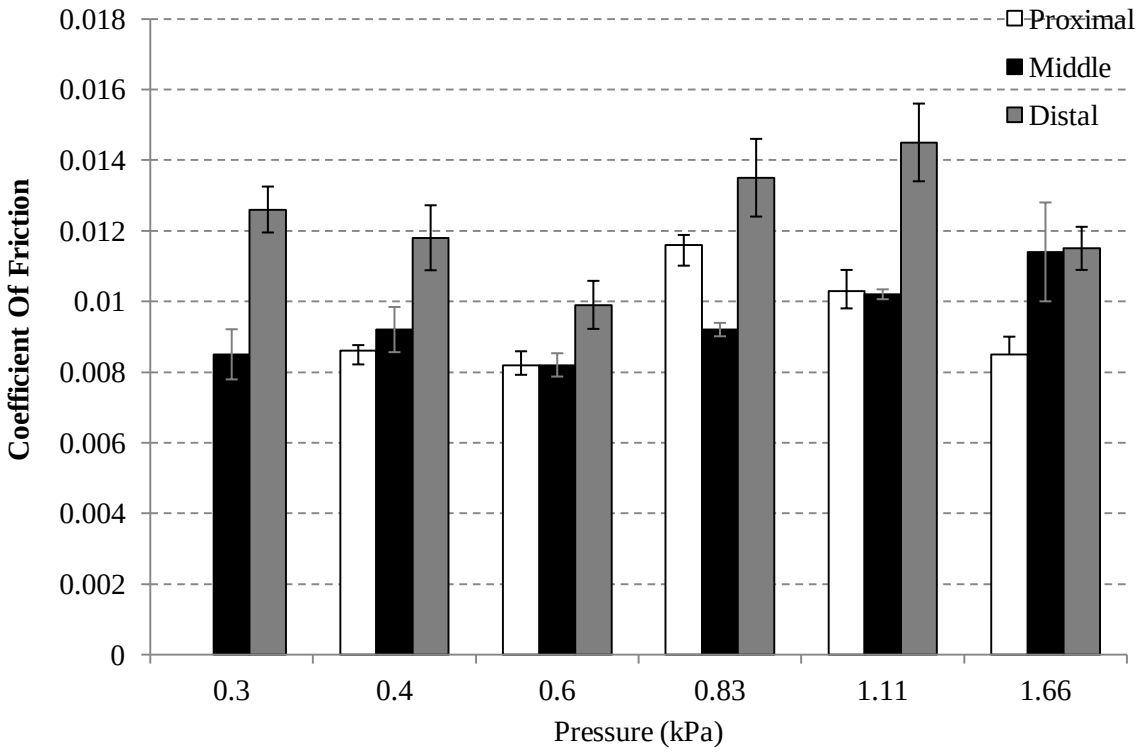

Figure 19. Coefficient of Friction for edgeless, polished stainless steel sled on small bowel mucosa; pressure results. Error bars represent a 95% confidence interval around the mean.

4.2.3 Velocity Results

The velocity study indicates that the friction force increases with increasing velocity. A single factor ANOVA was applied to compare differences in friction force versus velocity and the difference was found to be significant ($p < 0.05$). The data from measurements taken from the velocity test are shown in Figure 20.

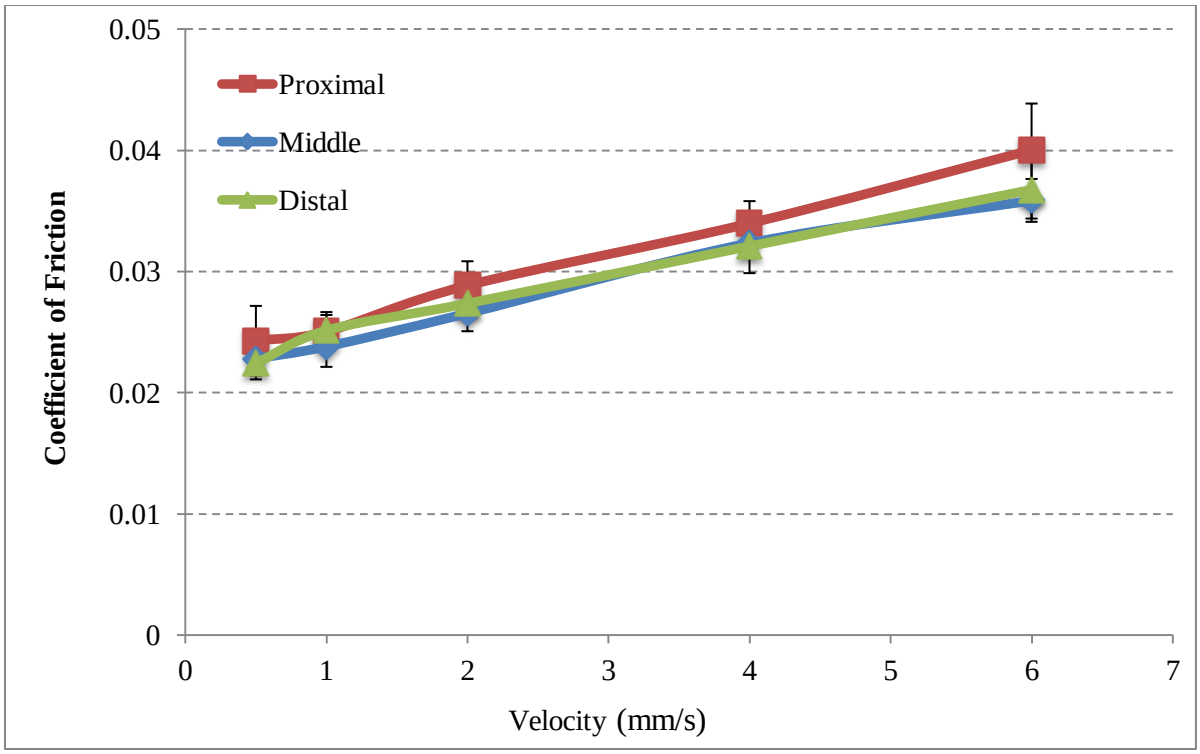

Figure 20. Coefficient of Friction for 0.94 N edgeless, polished stainless steel sled on small bowel mucosa: velocity results using pulley tribometer. Error bars represent a 95% confidence interval around the mean.

4.2.3 Validation of Pulley Tribometer System

A comparison of the magnitude of the friction force measured using the pulley and pure sliding tribometers showed that the tribometer systems could be considered equivalent. A representative data set, comparing the minimum and maximum sled speeds for the two systems on the middle section of small bowel mucosa is shown in Figure 21. The tests were conducted on two different pigs, so slight variations were expected, however for this comparison they were not significant. The error bars shown in Figure 21 represent a 95% confidence interval on a point estimate of the mean.

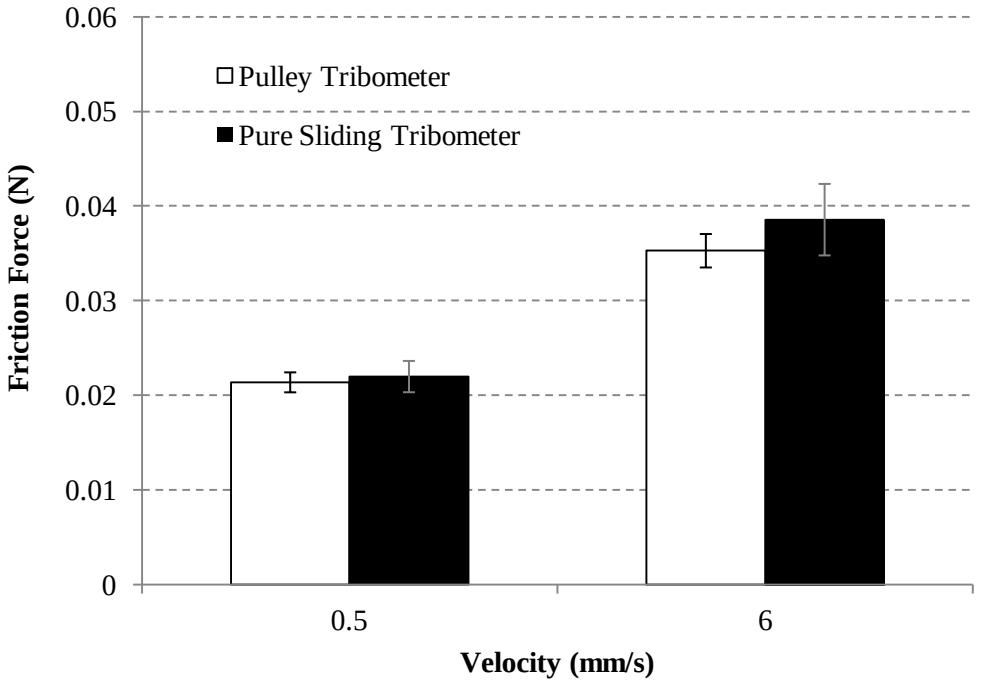

Figure 21. Comparison of pulley and pure sliding tribometer systems on middle section of small bowel mucosa. A 0.94 N edgeless, polished stainless steel sled was used. Error bars represent a 95% confidence interval around the mean.

4.3 Final Tribometer Design: Sled with Negligible Edge Effects

Following testing described in Section 3.3, the results of the experiments conducted with the inverted pure sliding tribometer device were analyzed with a 4-factor ANOVA. IBM's SPSS Statistics package was utilized for this analysis. As noted in Section 3.3, a fully crossed, mixed model factorial experiment was conducted. The significance level was set at 0.05 and both main and interaction effects were found to be significant, listed in Table 4. One main effect, material, was significant. However, there were also two- and four-way interactions, which required additional analysis to properly interpret the results.

Because the four-way interaction included a random factor, pig, it is possible to look at the fixed effects for each individual pig. Material was a significant factor, affecting the friction

response for each of the three pigs. Within Pig 1, in addition to material, there were two- and three-way interactions. In order to extract meaningful interpretations of this data, the importance

Table 4. Main effects, interactions and their associated p-values for parameters tested using inverted sled tribometer

Source Of Variation	p-value
Main Effects	
Material	0.045
2 Way Interactions	
Pig x Region	0.001
Pig x Material	0.000
Pig x Contact	0.004
4 Way Interactions	
Pig x Region x Material x Contact	0.019

of each significant effect was calculated, using (4), where $\widehat{\omega}^2$ is the importance, *SS* is the sum of squares, *MS* is the mean of squares and *df* is the degrees of freedom.

$$\widehat{\boldsymbol{\omega}}^{\mathbf{2}} = \frac{\boldsymbol{SS_{effects} - (MS_{residuals} * df)}}{\boldsymbol{SS_{total} - MS_{residuals}}} \quad (4)$$

Based on this calculation, it can be stated that 86.3% of the variability within Pig 1 is explained by knowing against which material the tissue was being tested. In total, from Pig 1, approximately 95.1% of the total variability could be explained by knowing specifics of the treatment combination. Table 5 shows the importance of the other significant effects from Pig 1. Further, when looking at material and contact area across the three regions of the small bowel, it was further possible to compare contact area and material. Figure 22, Figure 23, Figure 24 and Figure 25 highlight the differences and trends. Tukey's test was conducted to determine which

treatment combinations could be considered different and are shown in Table 6, along with mean COF.

Table 5. Summary ANOVA data: Pig 1

Source	Type III	df	Mean	F	Sig. (p)	ω^2
Region	374.450	2	187.225	1.636	.223	n/a
Material	85809.420	2	42904.710	374.795	.000	86.3%
Contact	1443.282	1	1443.282	12.608	.002	1.3%
Region * Material	1820.992	4	455.248	3.977	.017	1.4%
Region * Contact	3633.189	2	1816.595	15.869	.000	3.4%
Material * Contact	699.446	2	349.723	3.055	.072	n/a
Region * Material * Contact	3215.469	4	803.867	7.022	.001	2.8%
Error	2060.551	18	114.475			
Corrected Total	99056.800	35				95.1%

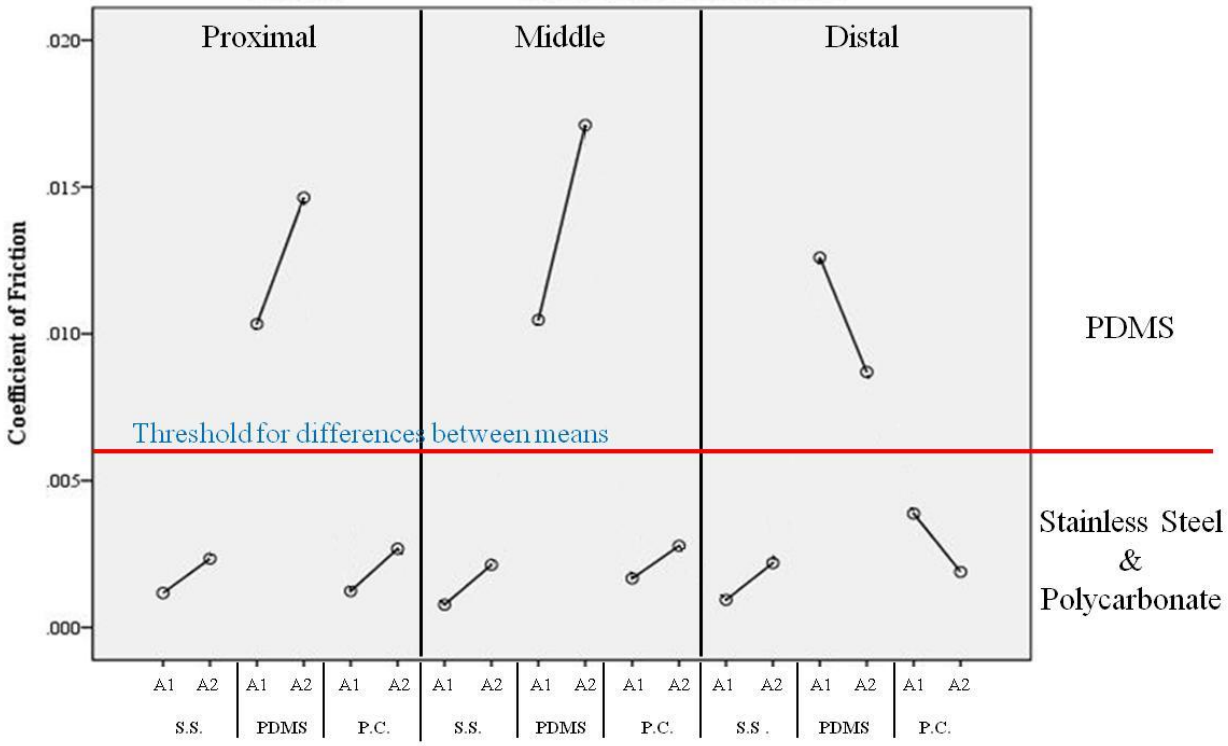

Figure 22. COF vs. treatment combination for Pig 1 (A1 = contact area 1, A2 = contact area 2; A1 < A2). The red line indicates a significance threshold between the means of the COF between small bowel and PDMS versus the COF between small bowel and both stainless steel and polycarbonate.

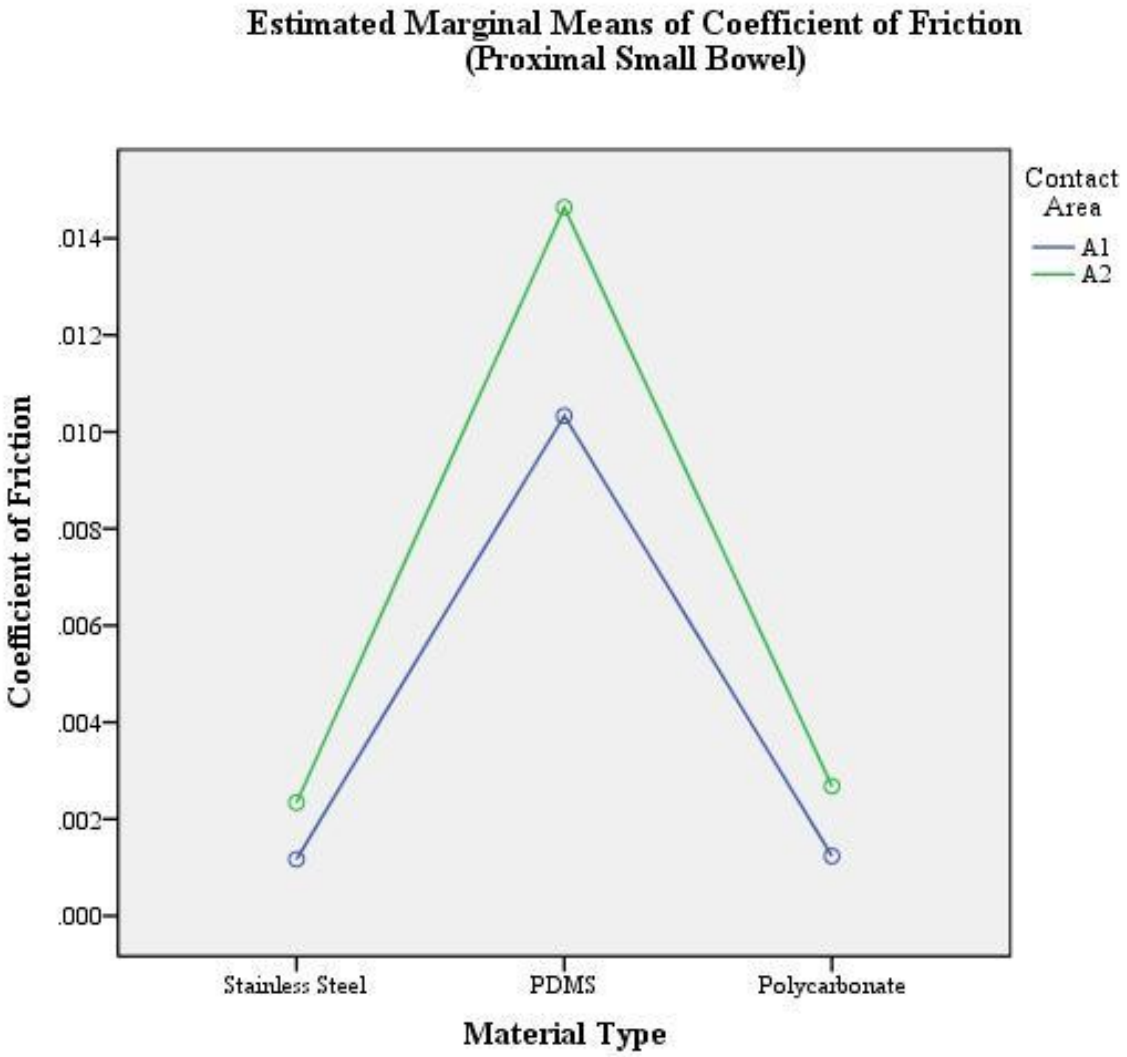

Figure 23. COF vs. treatment combination for Pig 1, proximal small bowel

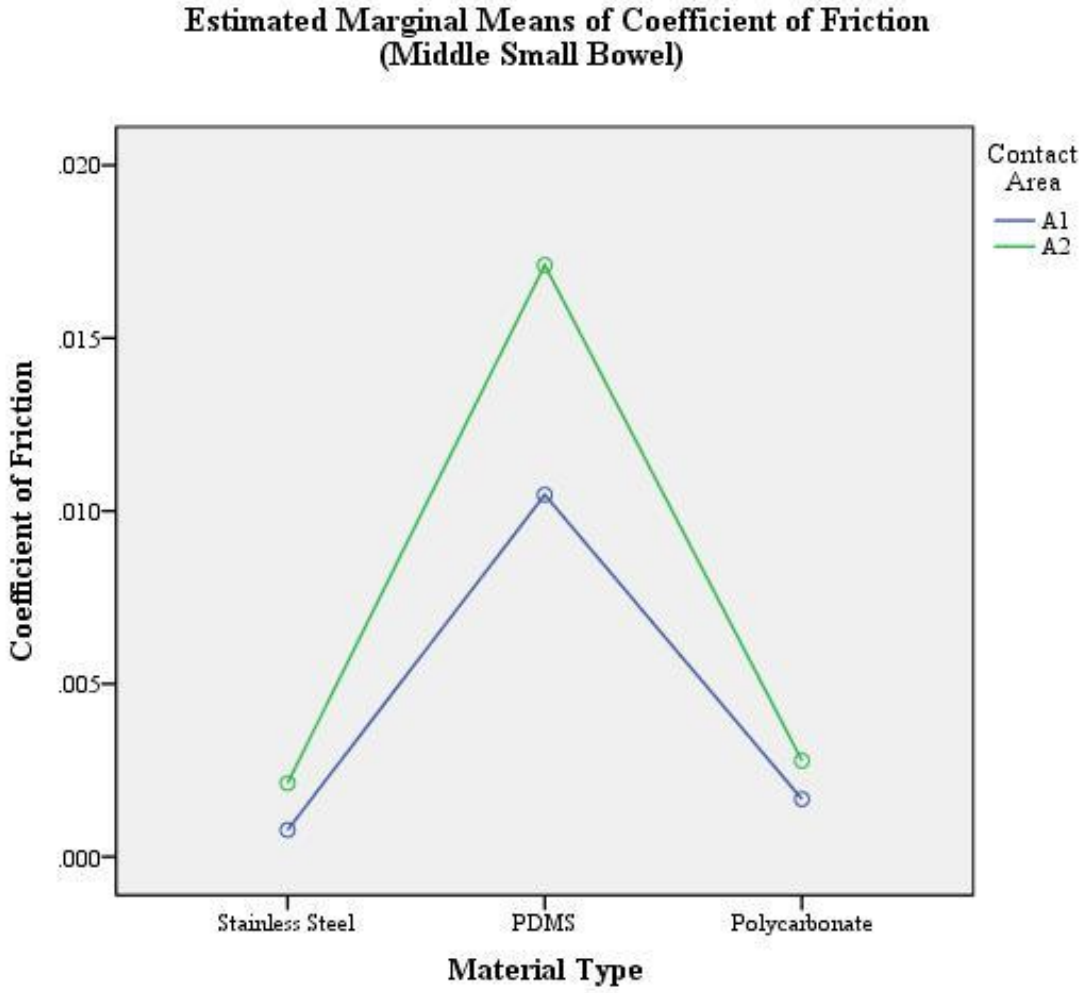

Figure 24. COF vs. treatment combination for Pig 1, middle small bowel

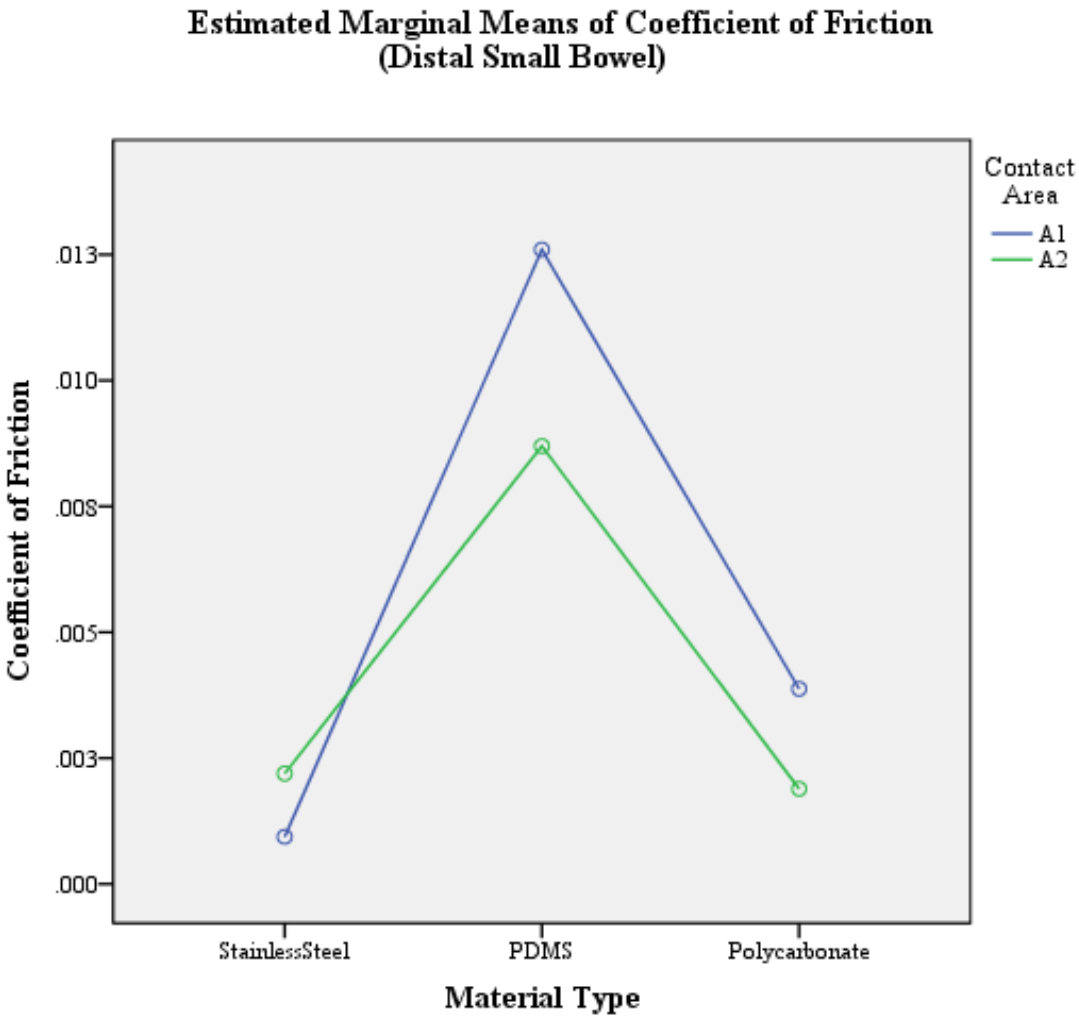

Figure 25. COF vs. treatment combination for Pig 1, distal small bowel

Table 6. COF values for equivalent treatment combinations, Pig 1

Material	Significant Region, Contact area	Mean COF
Stainless Steel	All Regions	0.002
PDMS	Distal , Contact area 2	0.01
PDMS	Middle, Contact area 1	0.013
PDMS	Proximal, Contact area 2	0.015
PDMS	Middle, Contact area 2	0.017

There were no interactions between factors for the remaining 2 pigs. Pig 2 and 3 had significant main effects from material and bowel region, indicating that mean friction coefficients could not be considered equal for each material nor region of the small bowel. Additionally, for Pig 2, the effect of contact area was significant. The explained variability was lower within these two pigs, with 57.3% and 42.1% total explained variability for Pig 2 and 3, respectively. The tables listing the significance and importance values for each the treatment effects for Pigs 2 and 3 can be found in Appendix H. Once again, Tukey's test was conducted to determine which of the means was different within each of the fixed factors. The results from Pigs 2 and 3 are graphically represented in Figure 26 and Figure 27, where the horizontal line transecting the plot indicates the threshold for differences in means. The comparisons of means for each pig are summarized as follows:

Pig 2:

$$\mu_{Proximal} = \mu_{Distal}$$

$$\mu_{Distal} = \mu_{Middle}$$

$$\mu_{Middle} < \mu_{Proximal}$$

$$\mu_{Stainless\ Steel} = \mu_{Polycarbonate} < \mu_{PDMS}$$

$$\mu_{Contact\ Area\ 1} < \mu_{Contact\ Area\ 2}$$

Pig 3:

$$\mu_{Proximal} = \mu_{Distal}$$

$$\mu_{Distal} = \mu_{Middle}$$

$$\mu_{Middle} < \mu_{Proximal}$$

$$\mu_{Stainless\ Steel} = \mu_{Polycarbonate} < \mu_{PDMS}$$

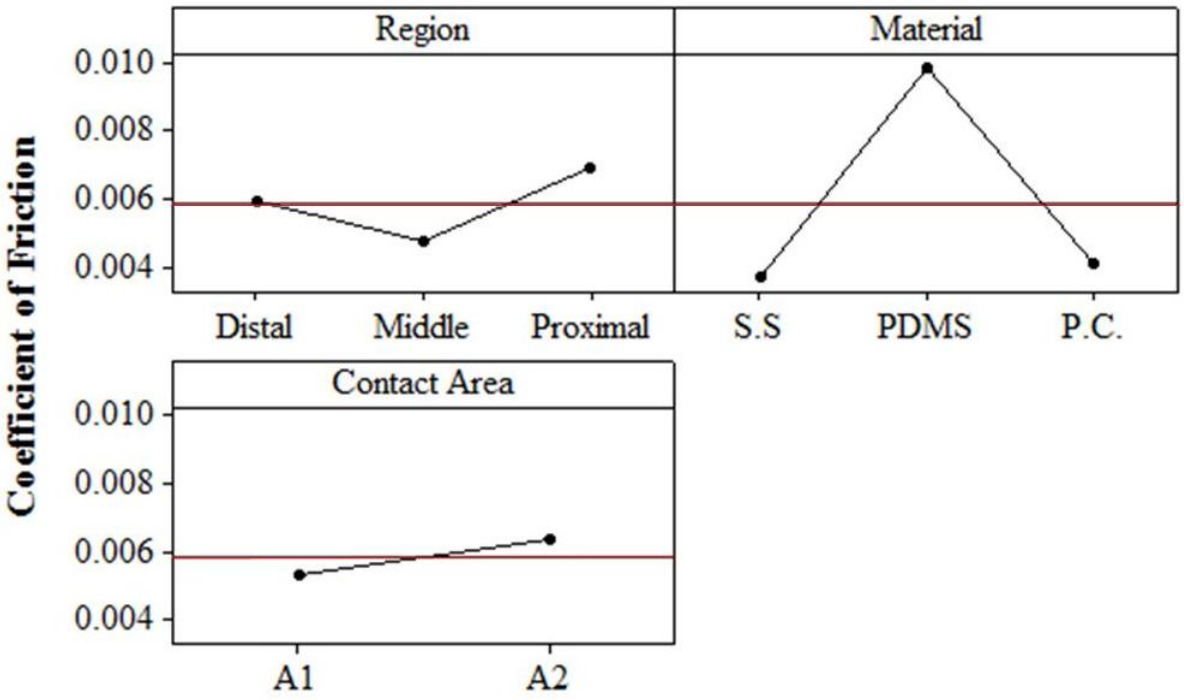

Figure 26. Comparison of Significant Effects, Pig 2

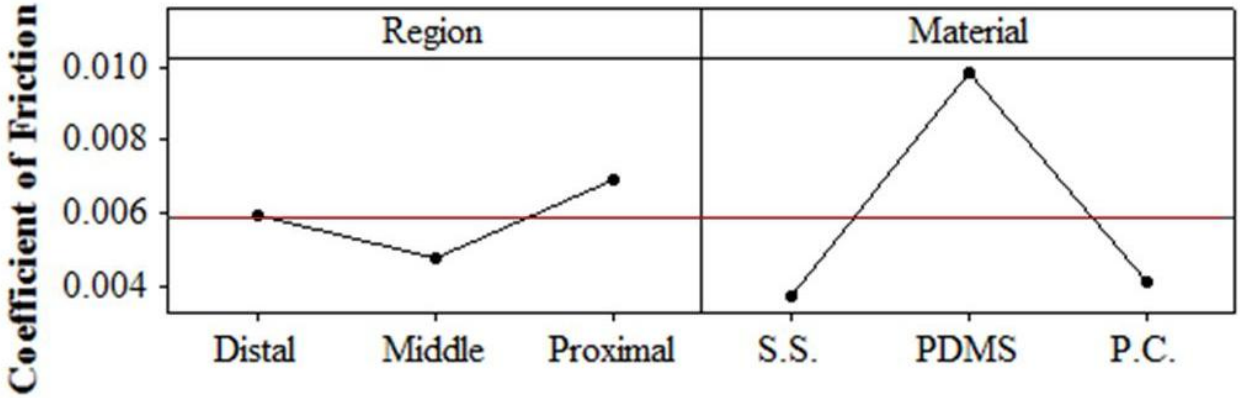

Figure 27. Comparison of Significant Effects, Pig 3

Chapter 5

Conclusions

The results implicate a number of factors which affect the friction response of small bowel lumen to a coupon moving upon it. In summary, the range of COF values that one can expect when testing any of the aforementioned parameters is between 0.0004 and 0.05. The range of friction forces varied from 0.001 to 0.086 N. This range of measured values is specific to the combination of testing parameters identified for this research, with added variability coming from within the testing animal population. While quite broad, a span of this size is likely analogous to what can be expected within the human population.

In particular, these results indicate that velocity and engineering material are two factors which affect the friction response most noticeably, depending upon which treatment level is being evaluated. It is also important to acknowledge that the friction force an RCE sees will vary depending upon which region of the bowel it is traveling within. Contact area and tissue condition also affect the friction force, although supplemental testing should be conducted to quantify this.

The results of the materials evaluation were as to be expected. PDMS yielded the highest COF due to the surface roughness induced by micropatterned PDMS pillars extending from the substrate. Due to equivalence in scale, PDMS columns likely interlock with the microvilli and this entanglement and adhesion requires more force to overcome as one surface passes over the other. In the case of polycarbonate and stainless steel, with reduced surface roughness, it is

possible that the mucus and high water content of the mucosal surface act as a lubrication layer, over which the opposing material can glide easily.

These results have important applications toward RCE design. Engineering material can be considered for parts of the capsule where high or low friction forces are desired. For example, shown in Figure 28, non-moving parts which experience pure sliding against the inner surface of the small bowel should be fabricated from materials such as stainless steel or polycarbonate, which were shown to have extremely low COF's when in contact with small bowel tissue. Segments of the RCE which are relied upon to achieve traction or high COF's could be coated with micro-patterned PDMS treads.

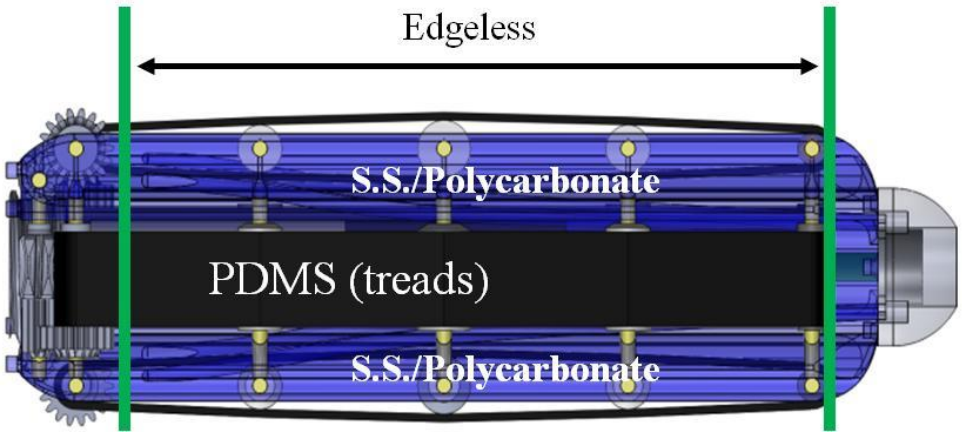

Figure 28. Potential RCE design with proposed material selections by component

The velocity results also have implications for RCE development. An important objective of the RCE is to reduce the duration of time for which the capsule endoscope is present with the patient's body. If the RCE's speed is to be increased, the designer should also be aware that the friction response of the small bowel lumen will increase correspondingly, which will require additional power to overcome. This can be readily seen by considering the work and power equations (5), (6), shown below, where x is the net distance travel, which in this case is the

length of the small bowel, *t* is time and *v* is the velocity of the RCE relative to the small bowel lumen surface.

$$Work = \int_C F_{friction} * dx = \int_C F_{friction} * vdt \quad (5)$$

$$Power = F_{friction} * v \quad (6)$$

We also saw that the friction response can vary depending on the location of the bowel. This can potentially be explained by considering the role of each section of the bowel during the digestion process. Dynamic changes in chemical composition, presence and size of food particulates and lumen surface characteristics distinguish the proximal from distal small bowel. The proximal bowel has larger fluctuations in pH and enzyme secretion and is responsible for physical mixing of larger food particles, whereas in the distal bowel the digestion processes are nearing completion and the environment can be considered more stable. When the RCE reaches the distal bowel it will likely encounter food debris, as was seen in the case of a pig despite fasting from solid food for a period of 48 hours prior to the study.

Finally, when considering *in situ* versus *in vitro* conditions, the results of this study indicate with some certainty that *in vitro* testing produces friction force values which are slightly higher than true *in vivo* conditions. However, due to deviations from true *in vivo* conditions, the results of this study cannot conclusively state what that magnitude truly is. The interpretation of these results point to a need to control the hydration and temperature of the tissue to replicate the *in vivo* state as closely as possible.

5.1 Future Work

To properly characterize the surface friction of the small bowel, the complex friction response to changes in sled weight must be fully distinguished. The friction forces and associated COF for an object in contact with the small bowel lumen is variable between runs, bowel regions and porcine models, so large sample sizes are required to reduce uncertainty. If a more accurate model of the bowel is to be constructed, weights, pressures and contact areas simulating realistic RCE parameters must be systematically evaluated. It will also be helpful to investigate the linearity of the friction versus velocity relationship over a broad range of testing speeds. As noted in the literature, there may be a maximum velocity above which the friction force begins to decrease, which could enhance the RCE's efficiency *in vivo* [37],[38],[41]. Finally, with any system that involves fluid, the role of the mucus layer interfacing with both the mucosa and external test object must be fully characterized and distinct contributions from the mucus layer and tissue surface must both be considered.

In conclusion, an RCE traversing within the small bowel with external controls will face a number of physical challenges. Mechanical forces from the intestinal wall and lumen surface are highly variable and dynamic. The COF range spans two orders of magnitude, and these values are much lower than engineers typically encounter in a system with the goal of controlled actuation. An RCE must be able to adapt to these conditions with optimized geometry and carefully selected materials. This research aims to assist with those design considerations.

References

[1] National Institutes of Health, 2009, "Burden of Digestive Diseases," U.S. Department of Health and Human Services.

[2] Hara A. K., Leighton J. A., Sharma V. K., and Fleischer D. E., 2004, "Small bowel: preliminary comparison of capsule endoscopy with barium study and CT," Radiology, 230(1), pp. 260–265.

[3] Froehlich F., Gonvers J. J., Vader J. P., Dubois R. W., and Burnand B., 1999, "Appropriateness of gastrointestinal endoscopy: risk of complications," Endoscopy, 31(8), pp. 684–686.

[4] Mayo Clinic staff, 2010, "Endoscopy: Risks - MayoClinic.com," Endoscopy. http://www.mayoclinic.com/health/endoscopy/MY00138/DSECTION=risks. Retrieved from web, 12 Apr, 2012.

[5] ASGE Technology Committee, 2011, "Report on Emerging Technology: GI Endoscopes," Gastrointestinal Endoscopy, 74(1).

[6] Bates, M.D R., 2010, "Complications From Screening Endoscopic Procedures Underestimated," EMaxHealth.

[7] Fernandes R., and Gracias D. H., 2009, "Toward a miniaturized mechanical surgeon," Materials Today, 12(10), pp. 14–20.

[8] Marmo R., Rotondano G., Piscopo R., Bianco M. A., and Cipolletta L., 2005, "Meta-analysis: capsule enteroscopy vs. conventional modalities in diagnosis of small bowel diseases," Alimentary Pharmacology & Therapeutics, 22(7), pp. 595–604.

[9] LePane C., Barkin J., Parra J., and Simon T., 2007, "Ulcerative Jejunoileitis: A Complication of Celiac Sprue Simulating Crohn's Disease Diagnosed with Capsule Endoscopy (PillCam)," Digestive Diseases and Sciences, 52(3), pp. 698–701.

[10] Hass D. J., 2012, "Detection of Crohn's Disease by Capsule Endoscopy," Visible Human Journal of Endoscopy, 11(1).

[11] Schwartz G., and Barkin J., 2007, "Small-Bowel Tumors Detected by Wireless Capsule Endoscopy," Digestive Diseases and Sciences, 52(4), pp. 1026–1030.

[12] McGee M. F., Rosen M. J., Marks J., Onders R. P., Chak A., Faulx A., Chen V. K., and Ponsky J., 2006, "A primer on natural orifice transluminal endoscopic surgery: building a new paradigm," Surg Innov, 13(2), pp. 86–93.

[13] Phee L., Accoto D., Menciassi A., Stefanini C., Carrozza M. C., and Dario P., 2002, "Analysis and development of locomotion devices for the gastrointestinal tract," Biomedical Engineering, IEEE Transactions on, 49(6), pp. 613 –616.

[14] Swain P., 2008, "The future of wireless capsule endoscopy," World Journal of Gastroenterology, 14(26), p. 4142.

[15] Sliker L. J., Kern M. D., Schoen J. A., and Rentschler M. E., 2012, "Surgical evaluation of a novel tethered robotic capsule endoscope using micro-patterned treads," Surgical endoscopy.

[16] H. Gregersen, and Kassab G. S., 2003, Biomechanics of the Gastrointestinal Tract: New Perspectives in Motility Research and Diagnostics, Springer, London.

[17] Gray, Henry, 1918. "XI. Splanchnology. 2g. The Small Intestine. Anatomy of the Human Body."

[18] Jensen, M.D. J., and Freese D., 2007, "Malabsorption Syndromes," Colorado Center for Digestive Disorders.
[19] Porter, M.D. R. S., and M.D. K., The Merck Manual Home Health Handbook.
[20] Guyton A., and Hall J., 2006, Textbook of Medical Physiology, Elsevier.
[21] Lai S. K., Wang Y.-Y., Wirtz D., and Hanes J., 2009, "Micro- and macrorheology of mucus," Adv Drug Deliv Rev, 61(2), pp. 86–100.
[22] Atuma C., Strugala V., Allen A., and Holm L., 2001, "The adherent gastrointestinal mucus gel layer: thickness and physical state in vivo," American Journal of Physiology - Gastrointestinal and Liver Physiology, 280(5), pp. G922 –G929.
[23] Terry B. S., Lyle A. B., Schoen J. A., and Rentschler M. E., 2011, "Preliminary mechanical characterization of the small bowel for in vivo robotic mobility," J Biomech Eng, 133(9), p. 091010.
[24] Terry B., Schoen J., and Rentschler M., "Measurements of the contact force from myenteric contractions on a solid bolus," Journal of Robotic Surgery, pp. 1–5.
[25] Terry B., Schoen J., and Rent M., 2011, "Characterization and Experimental Results of a Novel Sensor for Measuring the Radial Force from Myenteric Contractions," IEEE Transactions on Biomedical Engineering.
[26] Terry B., Schoen J., and Rentschler M., 2011, "Experimental Measurements of the Radial Force from Myenteric Contractions on a Solid Bolus," Journal of Surgical Endoscopy.
[27] Terry B. S., Passernig A. C., Hill M. L., Schoen J. A., and Rentschler M. E., "Small intestine Mucosal adhesivity to In vivo capsule robot materials," Journal of the Mechanical Behavior of Biomedical Materials, (0).
[28] Baek N.-K., Sung I.-H., and Kim D.-E., 2004, "Frictional resistance characteristics of a capsule inside the intestine for microendoscope design," Proceedings of the Institution of Mechanical Engineers, Part H: Journal of Engineering in Medicine, 218(3), pp. 193–201.
[29] Dario P., Ciarletta P., Menciassi A., and Kim B., 2004, "Modeling and experimental validation of the locomotion of endoscopic robots in the colon," INTERNATIONAL JOURNAL OF ROBOTICS RESEARCH, 23(4-5), pp. 549–556.
[30] Kim J.-S., Sung I.-H., Kim Y.-T., Kwon E.-Y., Kim D.-E., and Jang Y. H., 2006, "Experimental investigation of frictional and viscoelastic properties of intestine for microendoscope application," Tribol Lett, 22(2), pp. 143–149.
[31] Accoto D., Stefanini C., and Phee L., 2001, "Measurement of the frictional properties of the GI tract," Proceedings of the 2nd International Conference on Tribology, 1, pp. 153–158.
[32] Wang X., and Meng M. Q.-H., 2010, "An experimental study of resistant properties of the small intestine for an active capsule endoscope," Proc Inst Mech Eng H, 224(1), pp. 107–118.
[33] Yoshida H., and Tribology U. of L. I. of, 2003, Biological lubrication of hydrated surface layer in small intestine (from: Tribological research and design for engineering systems), Elsevier.
[34] Ringlein J., and Robbins M. O., 2004, "Understanding and illustrating the atomic origins of friction," American Journal of Physics, 72(7), p. 884.
[35] Unknown, "Introduction to Tribology – Friction."
[36] Olsson H., Astrom K., deWit C., Gafvert M., and Lischinsky P., 1998, "Friction Models and Friction Compensation," Eur. J. Control, 4(3), pp. 176–195.

[37] Grosch K. A., 1963, “The Relation between the Friction and Viscoelastic Properties of Rubber,” Proceedings of the Royal Society of London Series A. Mathematical and Physical Sciences, 274(1356), pp. 21–39.
[38] Ludema K. C., and Tabor D., September, “The friction and visco-elastic properties of polymeric solids,” Wear, 9(5), pp. 329–348.
[39] Bahadur S., and Ludema K. C., 1971, “The viscoelastic nature of the sliding friction of polyethylene, polypropylene and copolymers,” Wear, 18(2), pp. 109–128.
[40] Yamaguchi T., Ohmata S., and Doi M., 2009, “Regular to chaotic transition of stick–slip motion in sliding friction of an adhesive gel-sheet,” Journal of Physics: Condensed Matter, 21(20), p. 205105.
[41] Gong J. P., and Osada Y., 2002, “Surface friction of polymer gels,” Progress in Polymer Science, 27(1), pp. 3–38.
[42] Liao D.-H., Zhao J.-B., and Gregersen H., 2009, “Gastrointestinal tract modelling in health and disease,” World J Gastroenterol, 15(2), pp. 169–176.
[43] Lai S. K., Wang Y.-Y., Wirtz D., and Hanes J., 2009, “Micro- and macrorheology of mucus,” Adv Drug Deliv Rev, 61(2), pp. 86–100.
[44] Zhou D., 2004, “Study on Viscosity Property of GI mucus.”
[45] Mestecky J., Lamm M. E., Bienenstock J., McGhee J. R., Strober W., and Mayer L., Mucosal immunology, Academic Press.
[46] University of the Sciences in Philadelphia, 2005, Remington: the science and practice of pharmacy, Lippincott Williams & Wilkins, p 351.
[47] Kim Y.-T., 2006, “Frictional Behavior of Solid and Hollow Cylinders in contact against a porcine intestine specimen,” KSTLE International Journal, 7(2), pp. 51–55.
[48] Kim Y. T., and Kim D. E., 2007, “Biotribological Investigation of Multi-Tube Foot for Application in Medical Micro-Robot,” ASME Conf. Proc., 2007(48108), pp. 957–959.
[49] Wang K. D., and Yan G., 2008, “Research on measurement and modeling of the gastro intestine’s frictional characteristics,” Measurement Science and Technology, 20.
[50] Kwon J., 2005, “Bio-Material Property Measurement System for Locomotive Mechanism in Gastro-Intestinal Tract,” Proceedings of the 2005 IEEE International Conference on Robotics and Automation, Barcelona, Spain, pp. 1315–1329.
[51] Patterson J. K., Lei X. G., and Miller D. D., 2008, “The Pig as an Experimental Model for Elucidating the Mechanisms Governing Dietary Influence on Mineral Absorption,” Experimental Biology and Medicine, 233(6), pp. 651–664.
[52] Hoeg H. D., Slatkin A. B., Burdick J. W., and Grundfest W. S., 2000, “Biomechanical modeling of the small intestine as required for the design and operation of a robotic endoscope,” Robotics and Automation, 2000. Proceedings. ICRA ’00. IEEE International Conference on, pp. 1599–1606 vol.2.
[53] Munson B. R., Young D. F., Okiishi T. H., and Huebsch W. W., 2010, Fundamentals of Fluid Mechanics, John Wiley & Sons.
[54] Yim S., and Jeona D., 2009, “Capsular microrobot using directional friction spiral,” Proceedings of the 2009 IEEE international conference on Robotics and Automation, IEEE Press, Kobe, Japan, pp. 1022–1027.
[55] Sliker L. J., Wang X., Schoen J. A., and Rentschler M. E., 2010, “Micropatterned Treads for In Vivo Robotic Mobility,” Journal of Medical Devices, 4(4), p. 041006.

[56] Sliker L. J., and Rentschler M. E., 2012, “The Design and Characterization of a Testing Platform for Quantitative Evaluation of Tread Performance on Multiple Biological Substrates,” Biomedical Engineering, IEEE Transactions on, PP(99), p. 1.

Appendix A: Bill of Materials and Testing Equipment for Initial Tribometer Design

Table 7. Bill of materials for initial tribometer design (excluding hardware)

Part	Material
Tribometer base	Aluminum
Curved testing sled	Polycarbonate
Curved specimen tray	Aluminum
Specimen tray lift	Aluminum
Actuator mounts (2)	Aluminum
Load cell carriage	Aluminum
Linear slide	Aluminum (purchased)
Cable	Polymer string (purchased)

Table 8. Purchased hardware

Part	Supplier	Part No.
Limit switches (2)	McGuckin Hardware	VT16021C2
Load cell	Loadcell Central	ESP4-1KG
Motor driver	Sparkfun	ROB-09402
Linear Actuator	Haydon-Kerk	25844-05-001ENG
Data Acquisition Module	National Instruments	(NI USB 9237)
Data Acquisition Module	National Instruments	NI USB-6218
Data Acquisition Module	National Instruments	myDAQ

Appendix B: Part drawings for Initial Tribometer Design

Tribometer Base Plate

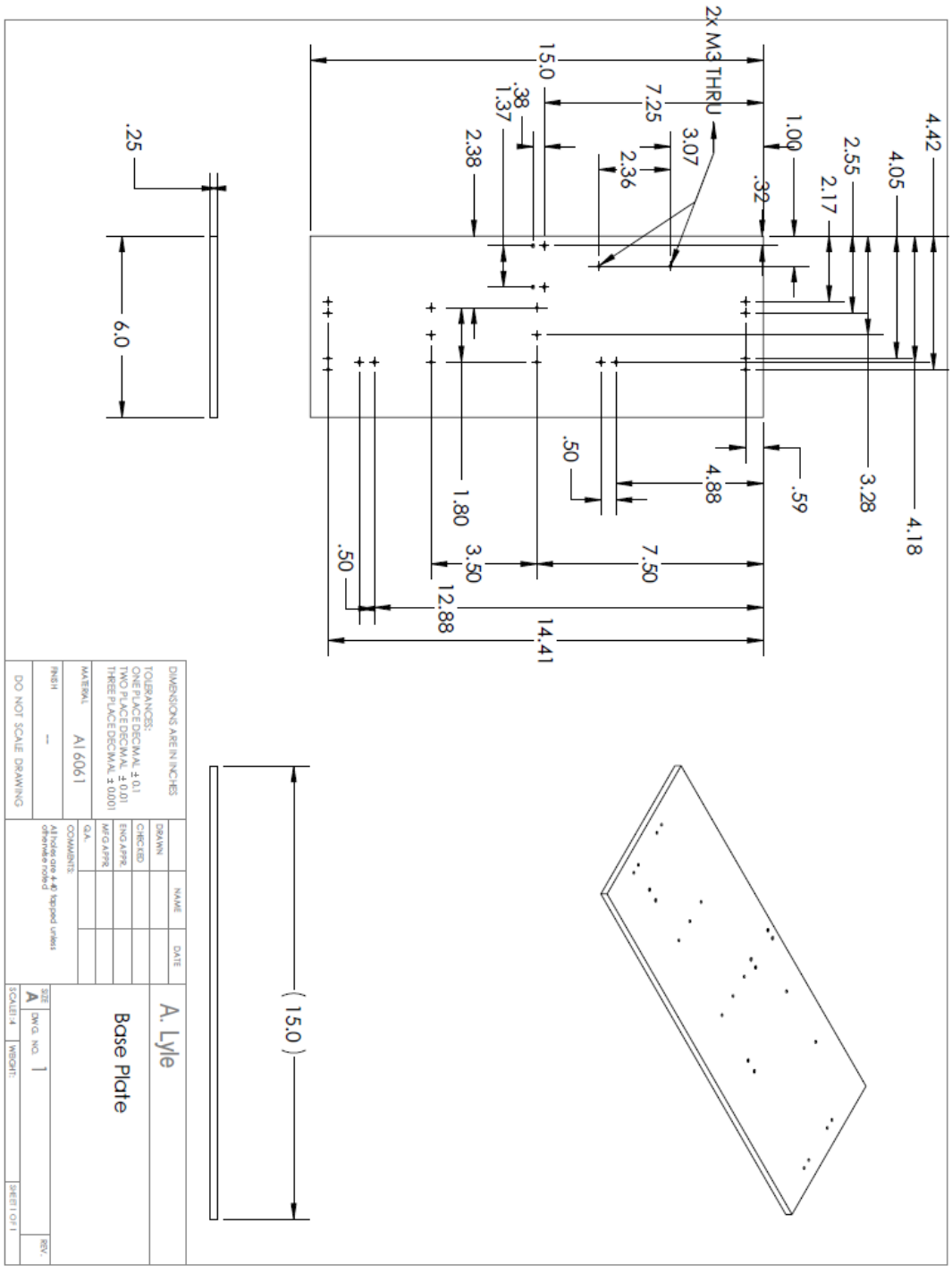

Tribometer Base Plate (zoom)

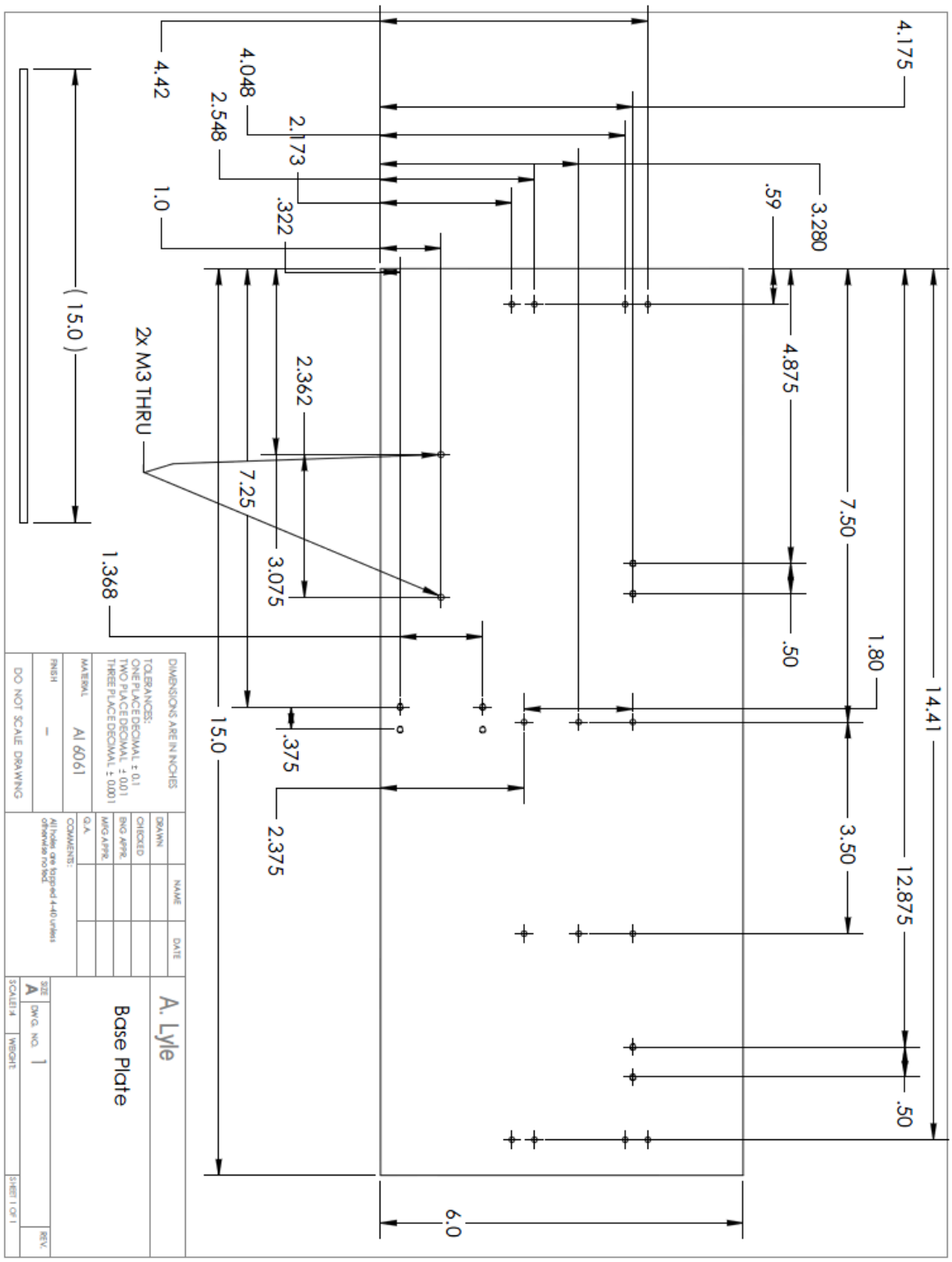

Curved Sled

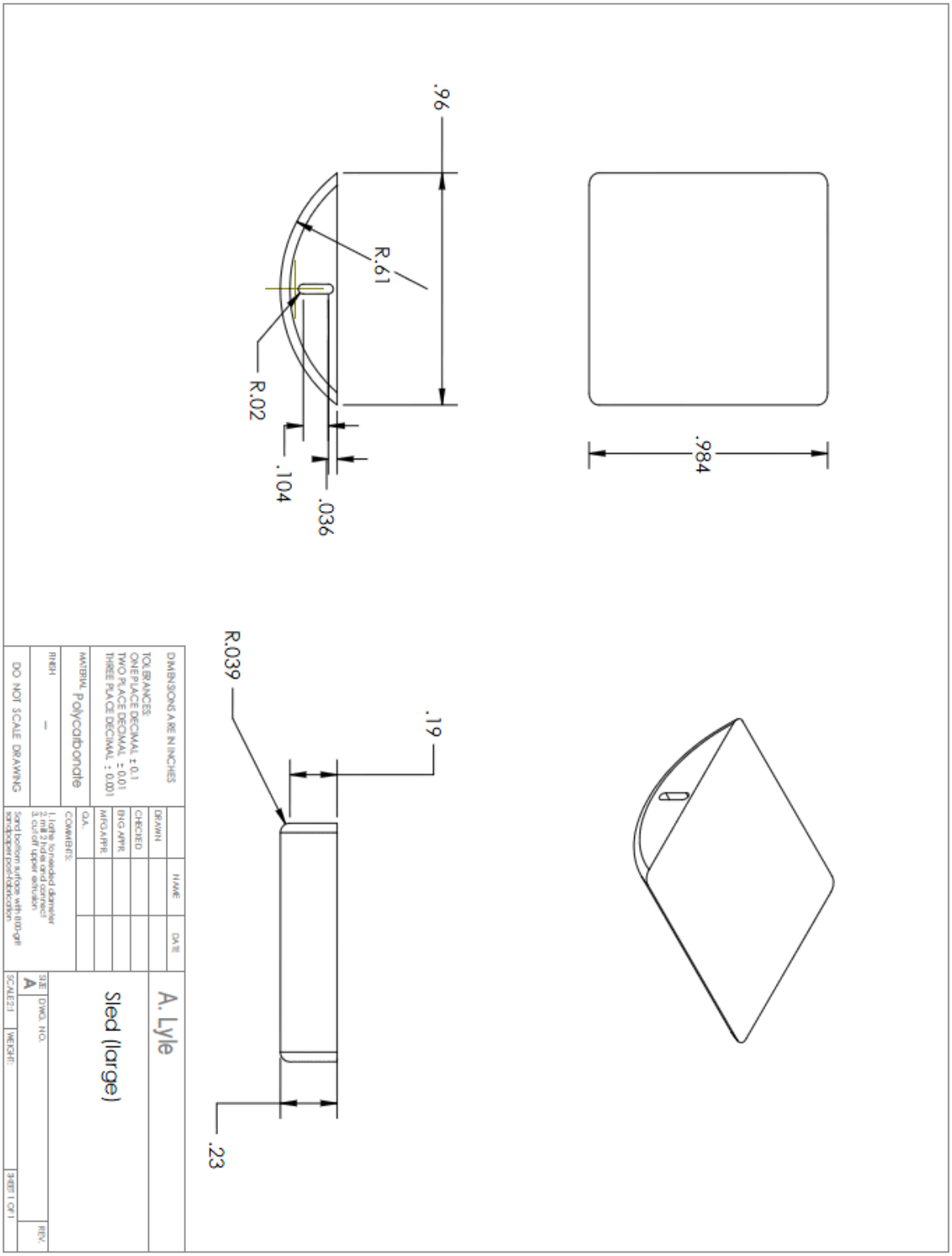
.96
R.61
R.02
.104
.036
.984
R.039
.19
.23
DIMENSIONS ARE IN INCHES
TOLERANCES:
ONE PLACE DECIMAL ± 0.1
TWO PLACE DECIMAL ± 0.01
THREE PLACE DECIMAL ± 0.001
MATERIAL Polycarbonate
FINISH –
DO NOT SCALE DRAWING
NAME
DATE
DRAWN
CHECKED
ENG APPR.
MFG APPR.
Q.A.
COMMENTS:
1. lathe to rescribed diameter
2. mill 2 holes and connect
3. cut off upper extrusion
Sand bottom surface with 600 grit sandpaper post-fabrication
A. Lyle
Sled (large)
SIZE
A
DWG. NO.
REV
SCALE:2:1
WEIGHT:
SHEET 1 OF 1

Curved Specimen Tray

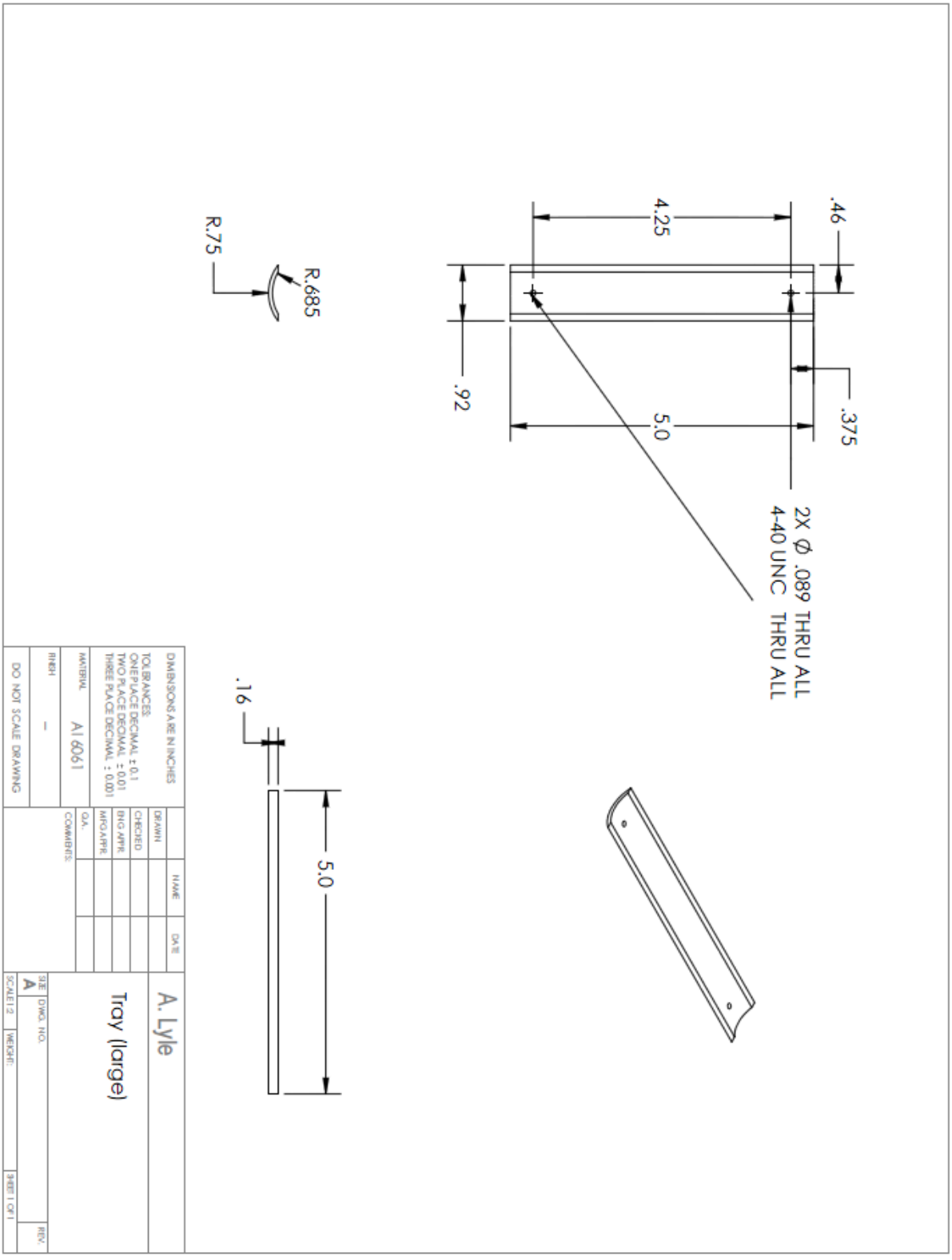

Tray lift (curved specimen tray)

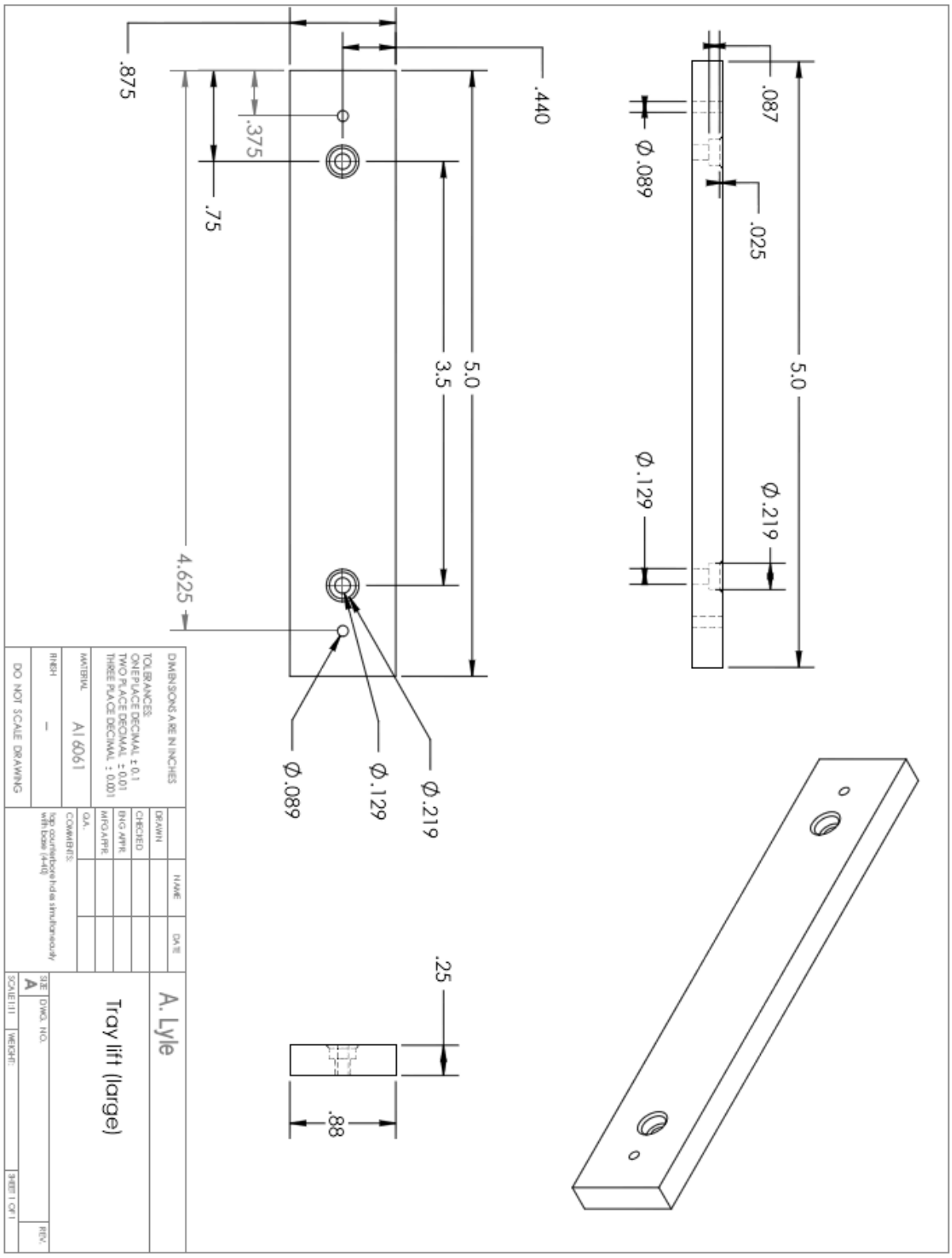

Actuator Mounts

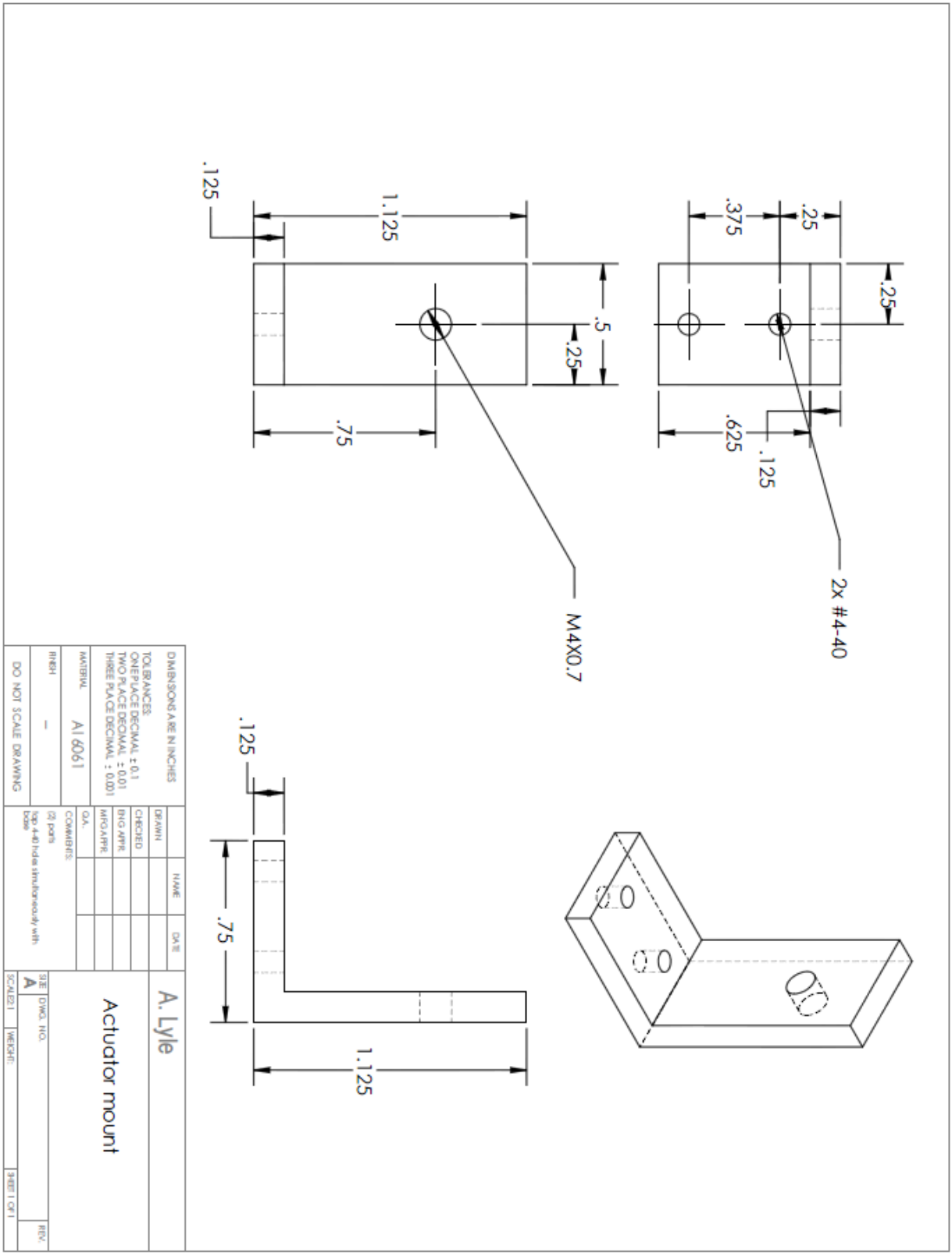

Load Cell Carriage/Mount

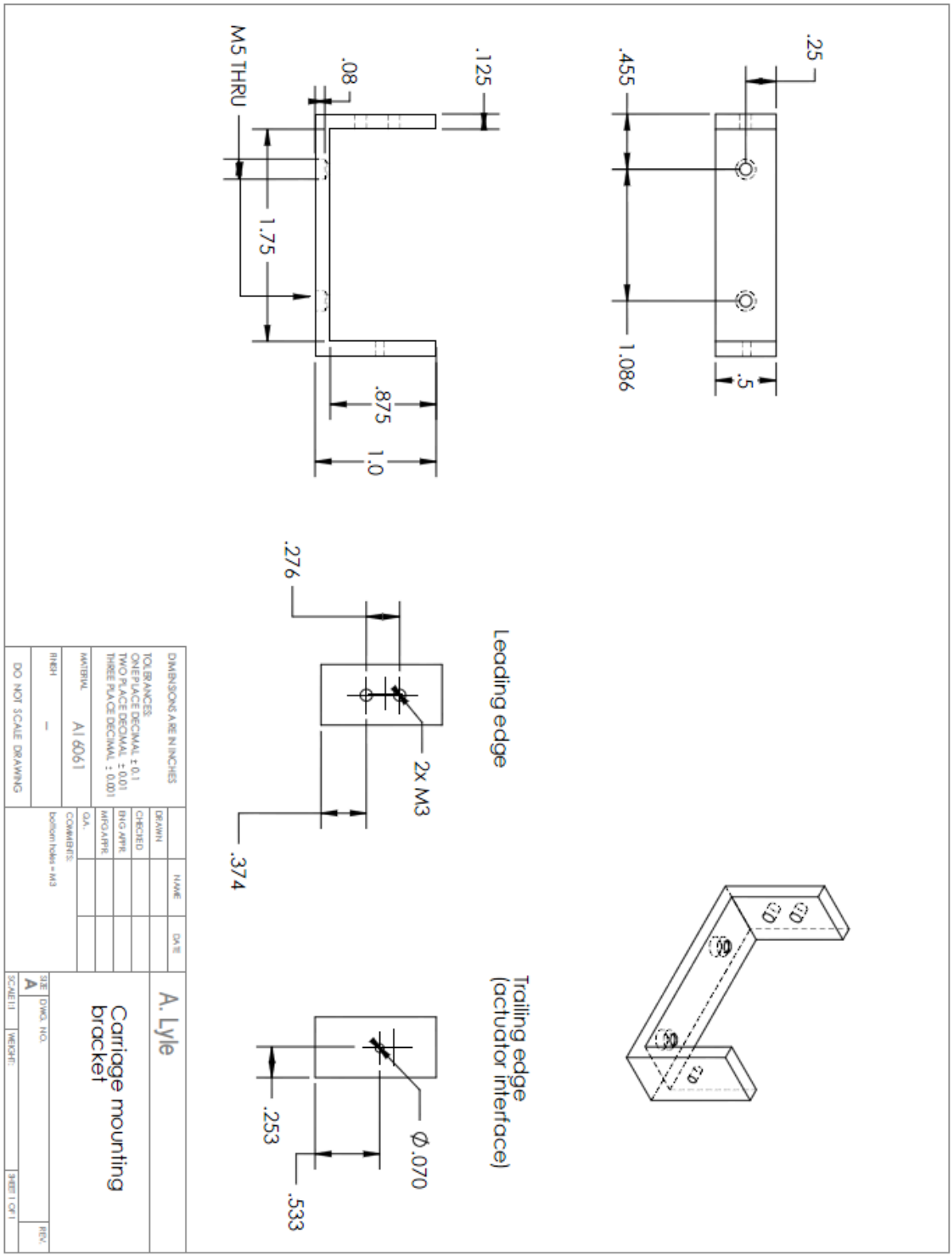

Appendix C: Load Cell Calibration

Rearranging (3) from Chapter 3 to solve for m, the calibration constant, where, *b* is an intercept, or voltage offset, variable *x* is considered to be the voltage output from the load cell and the *y*-term is the corresponding force on the load cell:

$$y = mx + b \tag{3}$$

$$m = \frac{y}{x} - b = \frac{Force}{Voltage} - offset \tag{8}$$

$$m = \frac{mass * acceleration}{load\ cell\ constant * excitation\ voltage} = \frac{1kg * \frac{9.81m}{s^2}}{\frac{1.1281mV}{V} * 5V} = 1{,}739\ \frac{N}{mV} \tag{9}$$

Table 9. Data points for load cell calibration

Weight (N)	Voltage (V)
0.3216621	3.73194E-05
0.6376598	7.32693E-05
1.0352719	0.000119009
1.4381754	0.000164075
1.913727	0.000219056
2.3969607	0.000274218
2.9603078	0.000338566
3.522205	0.000403755
4.6599688	0.000533507
6.2044552	0.000710338
9.4908052	0.001091825

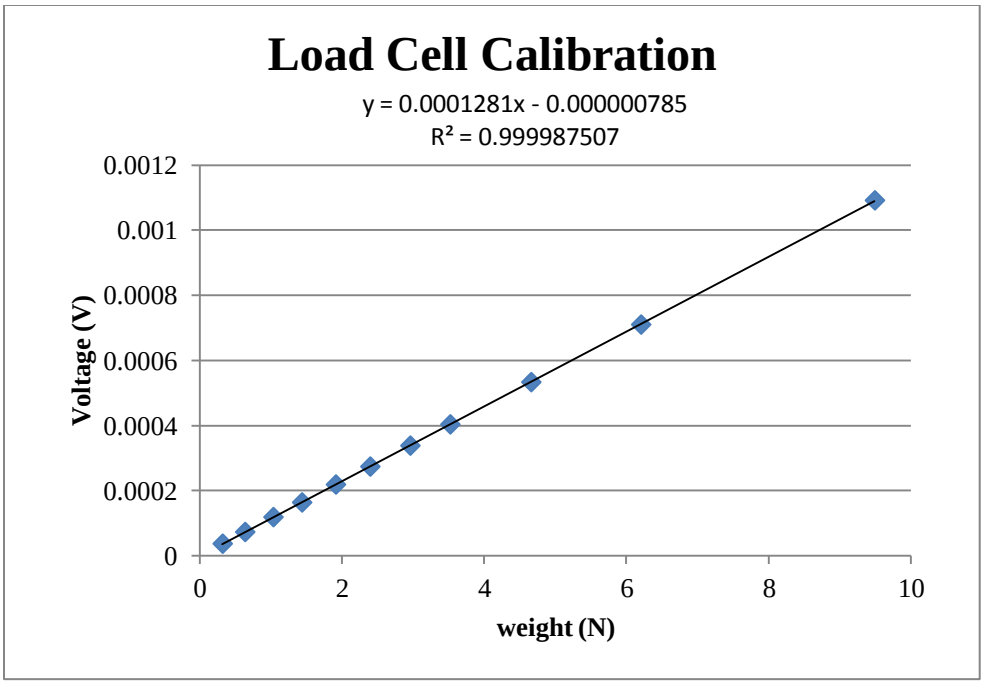

Figure 29. Least Squares Regression fit to acquire load cell calibration constant from emperical calibration test

Appendix D: Bill of Materials for Revised Tribometer Design (Edgeless sled)

Table 10. Bill of materials for revised tribometer design (edgeless sled) (excluding hardware)

Part	Material
Edgeless sled	Stainless steel
Cable	Polymer string
Specimen platform	Aluminum
Linear slide	Aluminum
Load cell carriage	Aluminum
Motor mounts (2)	Aluminum
Pulley (2)	Oil impregnated brass
Pulley mounts (2)	Aluminum
Pulley rods (2)	Stainless steel
Tribometer base	Aluminum

Table 11. Purchased hardware

Part	Supplier	Part No.
Limit switches (2)	McGuckin Hardware	VT16021C2
Load cell	Loadcell Central	ESP4-1KG
Motor driver	Sparkfun	ROB-09402
Linear Actuator	Haydon-Kerk	25844-05-001ENG
Data Acquisition Module	National Instruments	(NI USB 9237)
Data Acquisition Module	National Instruments	NI USB-6218
Data Acquisition Module	National Instruments	myDAQ

Appendix E: Part drawings for Edgeless Sled Tribometer Design

Edgeless, Overhanging Sled

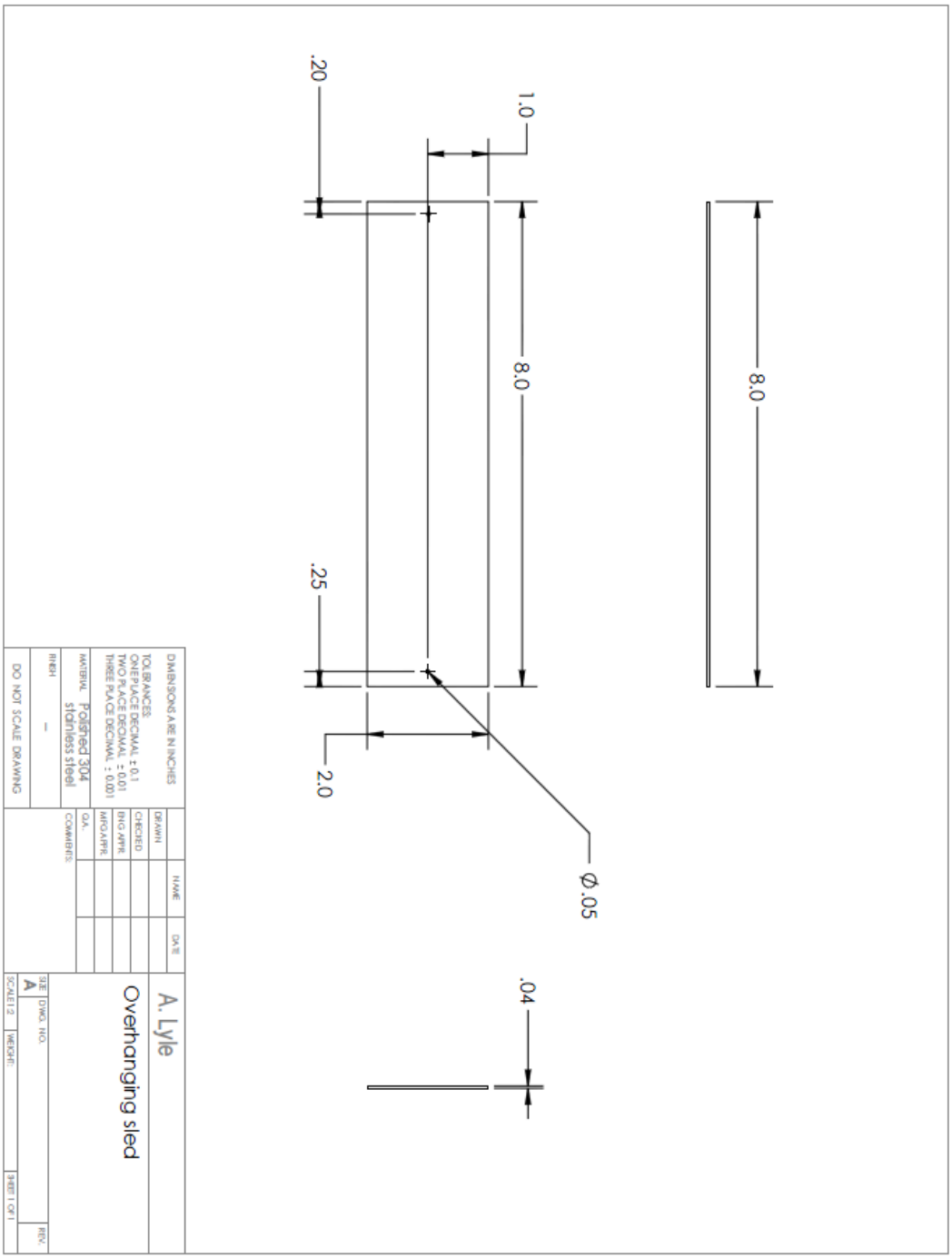

Specimen Tray lift

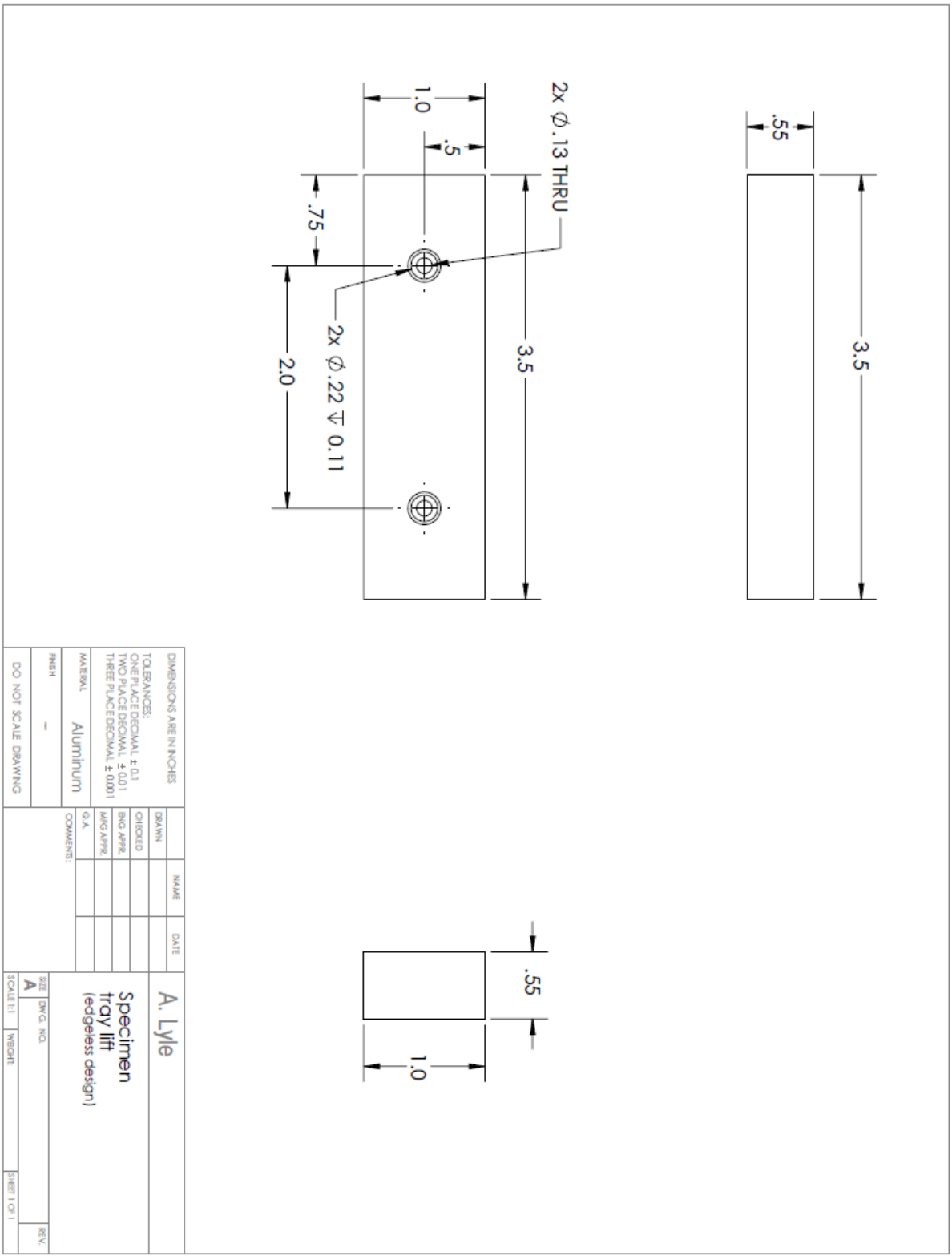

Pulley Mount

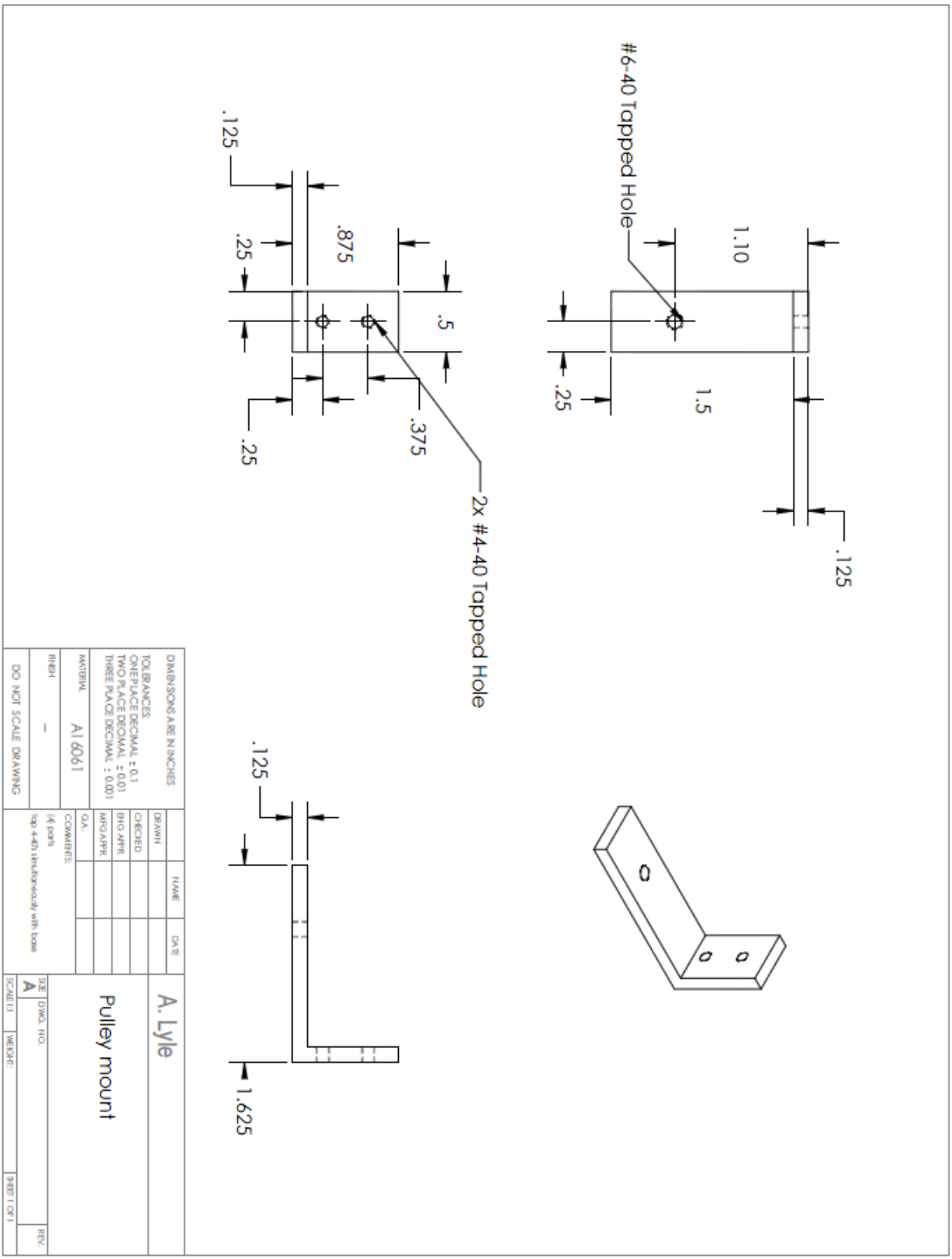

Pulley Rod

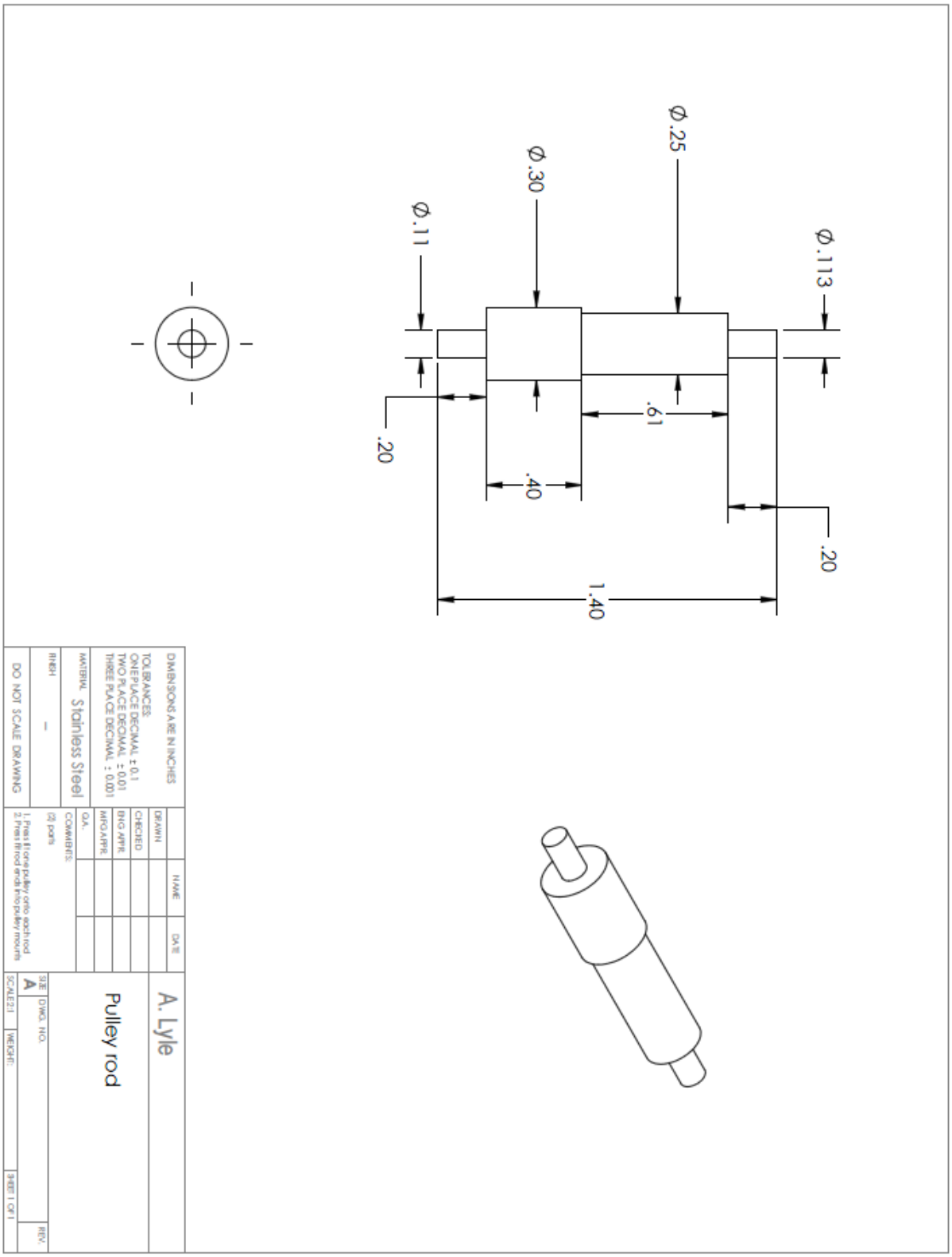
Ø.113
Ø.25
Ø.30
Ø.11
.61
.40
.20
.20
1.40
DIMENSIONS ARE IN INCHES
TOLERANCES:
ONE PLACE DECIMAL ± 0.1
TWO PLACE DECIMAL ± 0.01
THREE PLACE DECIMAL ± 0.001
MATERIAL Stainless Steel
FINISH –
DO NOT SCALE DRAWING
DRAWN
CHECKED
ENG APPR.
MFG APPR.
Q.A.
COMMENTS:
(2) parts
1. Press fit rod-pulley onto each rod
2. Press fit rod ends into pulley mounts
NAME
DATE
A. Lyle
Pulley rod
SIZE
A
DWG. NO.
REV
SCALE:2:1
WEIGHT:
SHEET 1 OF 1

Appendix F: Bill of Materials for Final Tribometer Design

Table 12. Bill of materials for final tribometer design (excluding hardware)

Part	Material
Test material plank	Stainless steel
Cable	Polymer string
Specimen fixture (2)	Aluminum
Specimen clamp (2)	Aluminum
Magnets for specimen clamp	
Linear slide	Aluminum
Load cell carriage	Aluminum
Motor mounts (2)	Aluminum
Pulley (2)	Oil impregnated brass
Pulley mounts (2)	Aluminum
Pulley rods (2)	Stainless steel
Tribometer base	Aluminum

Table 13. Purchased hardware

Part	Supplier	Part No.
Limit switches (2)	McGuckin Hardware	VT16021C2
Load cell	Loadcell Central	ESP4-1KG
Motor driver	Sparkfun	ROB-09402
Linear Actuator	Haydon-Kerk	25844-05-001ENG
Data Acquisition Module	National Instruments	(NI USB 9237)
Data Acquisition Module	National Instruments	NI USB-6218
Data Acquisition Module	National Instruments	myDAQ

Appendix G: Part Drawings for Final Tribometer Design (tissue fixtures)

Tissue Fixture for Contact Area 1 (2" x 0.5")

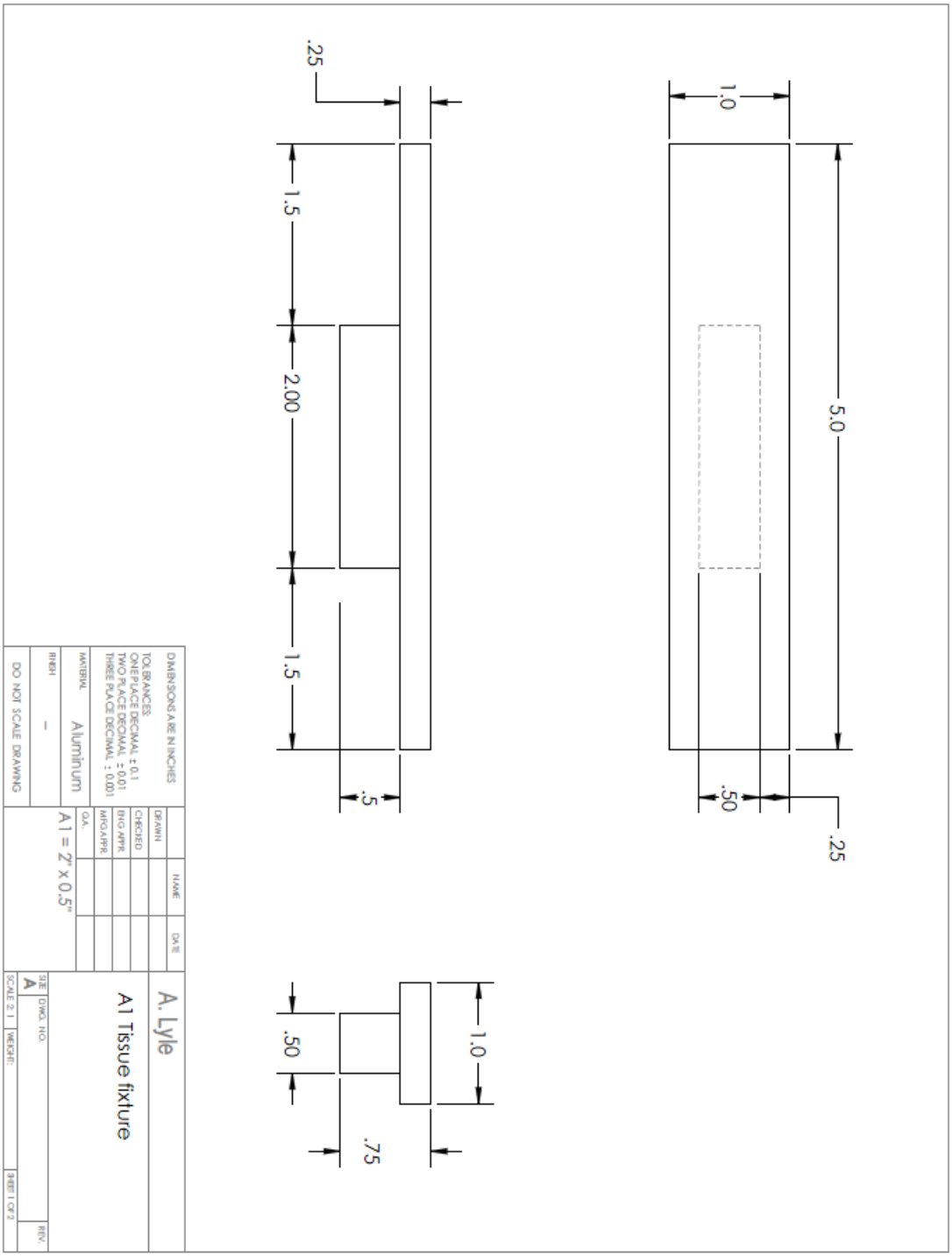

Clamping Plate for Contact Area 1 (2" x 0.5")

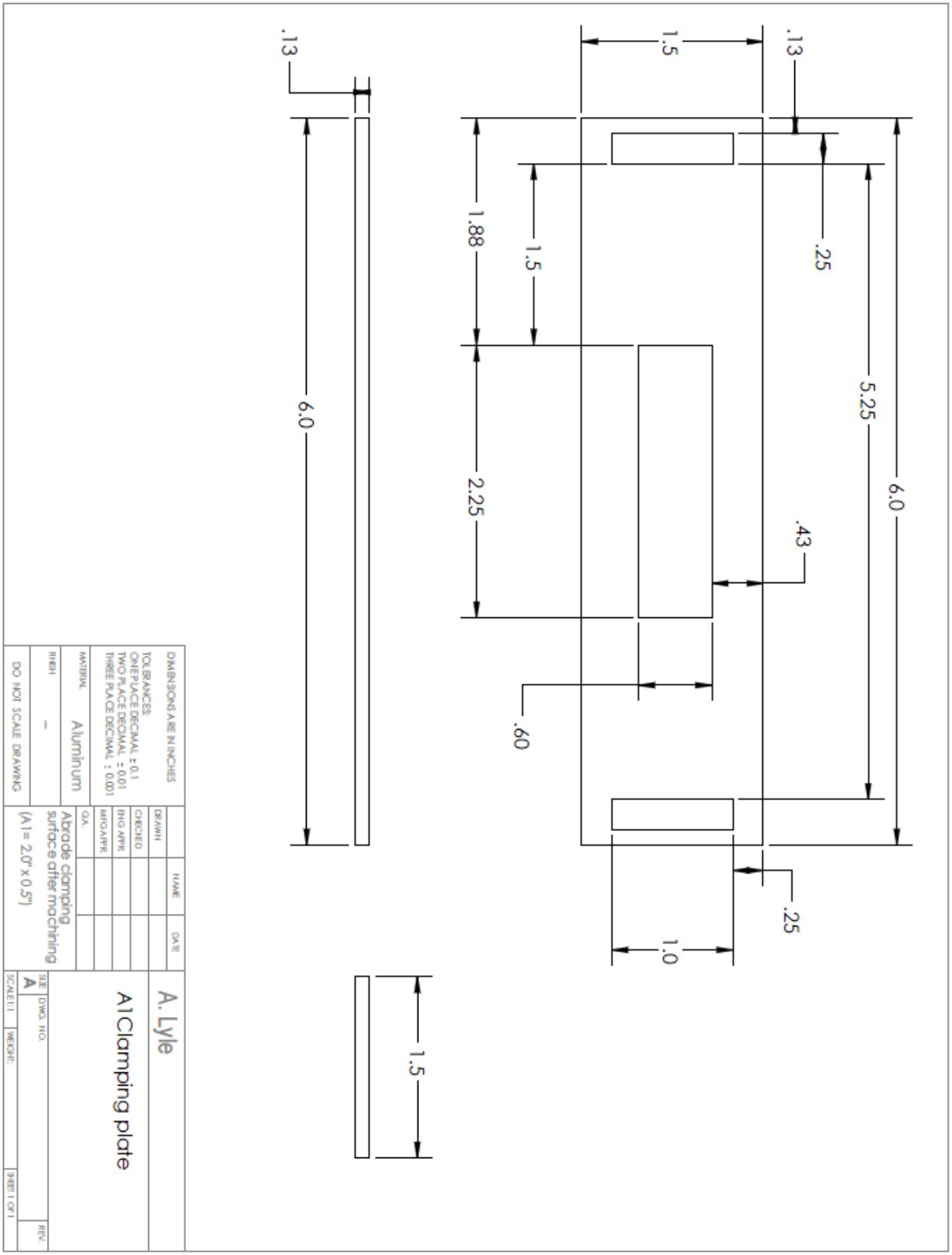

Tissue Fixture for Contact Area 2 (4" x 0.5")

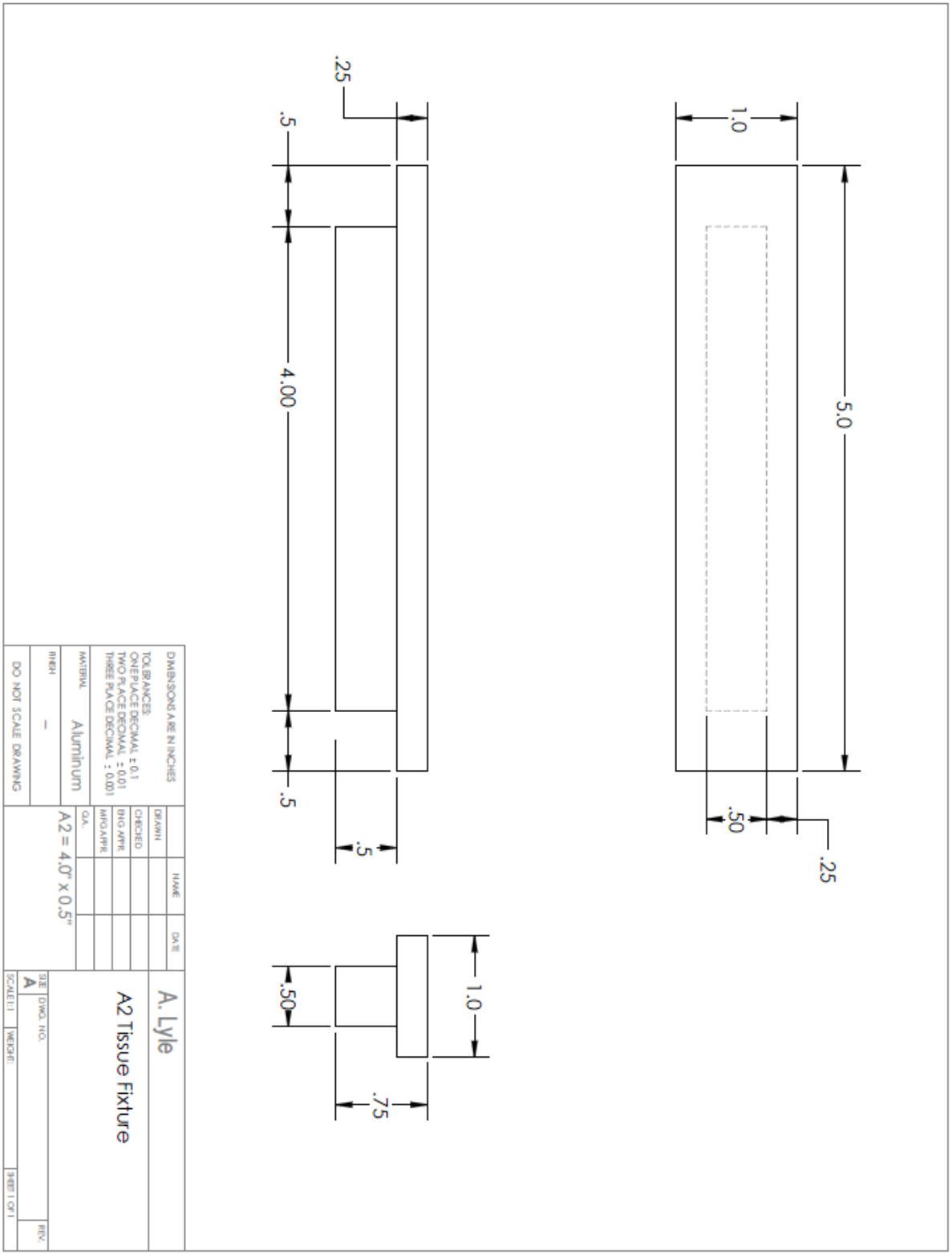

Clamping Plate for Contact Area 2 (4" x 0.5")

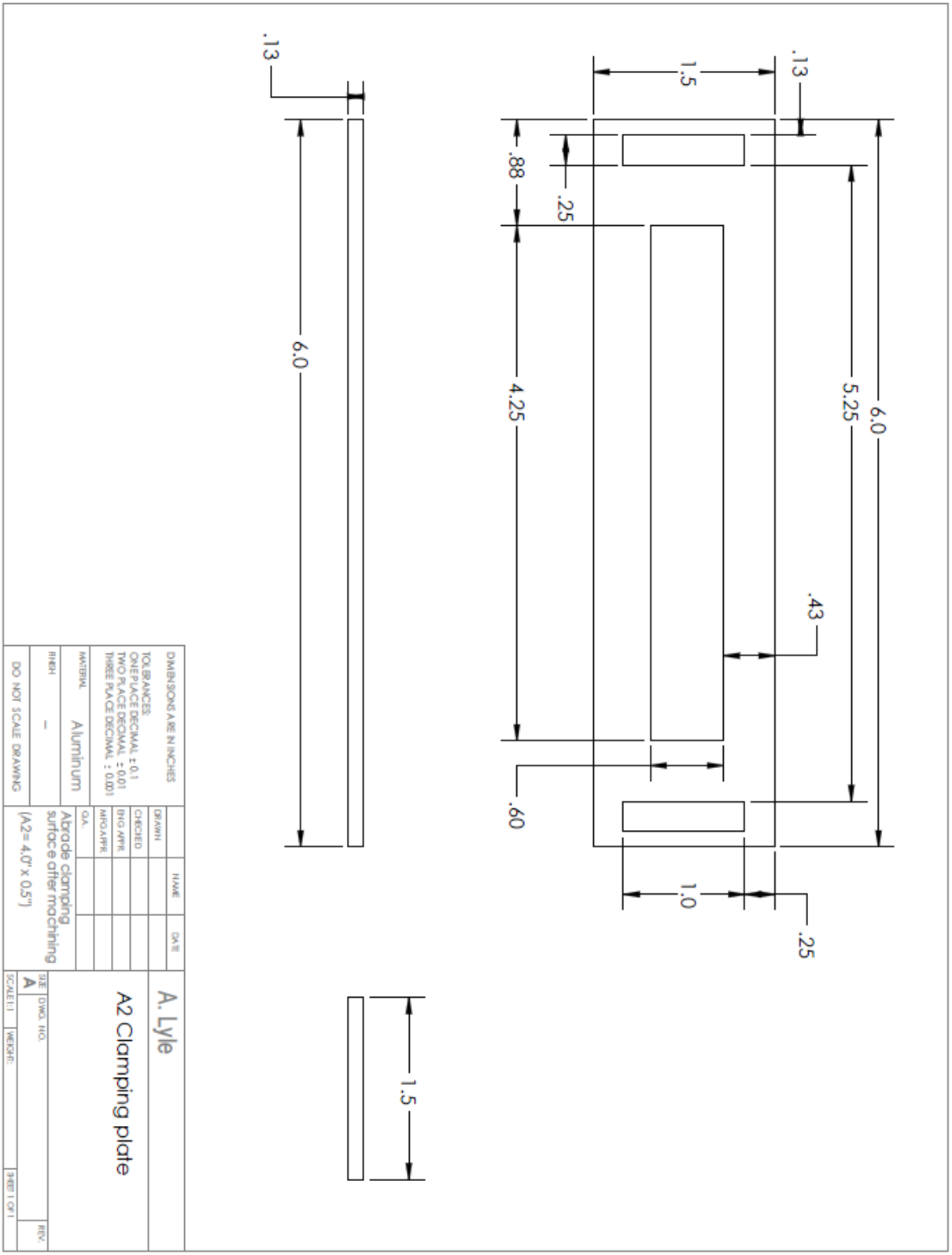

Appendix H: ANOVA Results from Final Experiment

Table 14. Summary ANOVA data: Pig 2

Source	Type III Sum	df	Mean	F	Sig.(p)	ω^2
Region	14143.527	2	7071.763	10.476	.001	25%
Material	12874.772	2	6437.386	9.536	.001	22.6%
Contact	5652.283	1	5652.283	8.373	.010	9.7%
Region * Material	1581.954	4	395.489	.586	.677	n/a
Region * Contact	163.818	2	81.909	.121	.886	n/a
Material * Contact	18.148	2	9.074	.013	.987	n/a
Region * Material * Contact	3845.739	4	961.435	1.424	.266	n/a
Error	12150.516	18	675.029			
Corrected Total	50430.758	35				57.3%

Table 15. Summary ANOVA data: Pig 3

Source	Type III Sum	df	Mean	F	Sig. (p)	ω^2
Region	3274.811	2	1637.406	4.246	.031	8.7%
Material	10404.888	2	5202.444	13.491	.000	33.4%
Contact	472.202	1	472.202	1.225	.283	n/a
Region * Material	2643.893	4	660.973	1.714	.191	n/a
Region * Contact	499.797	2	249.898	.648	.535	n/a
Material * Contact	341.351	2	170.676	.443	.649	n/a
Region * Material * Contact	3846.737	4	961.684	2.494	.080	n/a
Error	6941.181	18	385.621			
Corrected Total	28424.860	35				42.1%